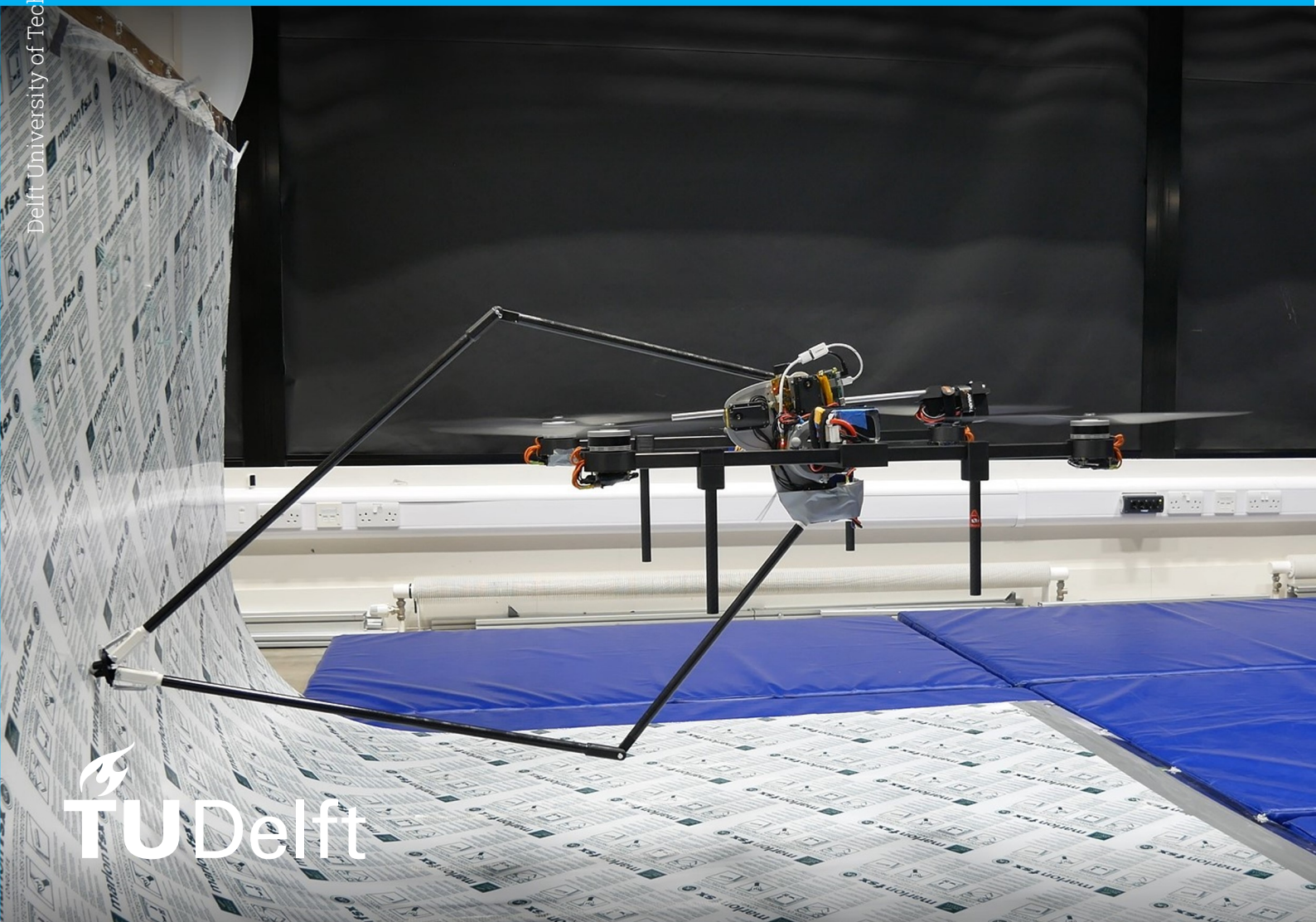


Sensorless Impedance Control for Curved Surface Inspections Using the Omni-Drone Aerial Manipulator

Hani Abu-Jurji



Sensorless Impedance Control for Curved Surface Inspections Using the Omni-Drone Aerial Manipulator

by

Hani Abu-Jurji

to obtain the degree of Master of Science
in the profile of Control & Simulation at the Faculty of Aerospace Engineering
at the Delft University of Technology,
to be defended publicly on Monday September 19, 2022 at 10:00.

Student number: 5284872
Project duration: October 1, 2021 – September 19, 2022
Thesis committee: Prof. dr. F. Scarano, TU Delft, committee chair & external examiner
Asst. Prof. S. Hamaza, TU Delft, supervisor
Asst. Prof. E.J.J. Smeur, TU Delft, internal examiner

An electronic version of this thesis is available at <http://repository.tudelft.nl/>.

Preface

The following thesis was written to obtain my Master degree in the profile of Control & Simulation at the Faculty of Aerospace Engineering at Delft University of Technology. The subject of the following work pertains to the design, implementation, and control of a novel aerial manipulator, named Omni-Drone. The inspiration comes from an earlier work by my supervisor, Asst. Prof. Salua Hamaza, along with Prof. Mirko Kovac of Imperial College London. There they had proposed the concept of an unmanned aerial vehicle (UAV) equipped with a rotating parallel manipulator for the purpose of contact-based inspection tasks. The work of this thesis expands on this concept by constructing the Omni-Drone aerial manipulator and implementing a control strategy based on onboard force estimation for a sensorless impedance controller. The goal is to demonstrate the capability of the novel aerial manipulator to perform contour following tasks of curved surfaces. Both stationary and aerial experiments were conducted using the system. The stationary experiments demonstrate the on-board estimator's effectiveness at accurately tracking the applied force at the end-effector as it is dynamically loaded and unloaded. Flight experiments then show adequate contour following of a curved surface through the use of the impedance controller.

This thesis will be publicly presented and defended in front of a committee consisting of Prof.dr. F. Scarano, Asst. Prof. S. Hamaza, and Asst. Prof. E.J.J. Smeur. on September 19, 2022.

I am extremely grateful to my supervisor, Asst. Prof. S. Hamaza, in particular for her continued extensive support throughout the past year in helping me achieve this milestone.

Many thanks to Yunus Govdeli and Oscar Pang at Imperial College London for their technical help during the experiment phase of this thesis.

I could not have undertaken this journey without the support of my family. Words cannot express my gratitude to my parents, Mervat & Saadallah Abu-Jurji, for providing me with the opportunities to pursue my education and for supporting me along the way. I am also extremely grateful to Zeina Abu-Jurji for her enormous continued encouragement and for being a wonderful sister to me.

Special thanks to Sylvester Bawab & Laura Seitova for taking me into their home for the past two years and giving me the support to complete this degree.

Lastly, but certainly not least, I would like to express my deepest appreciation to my wonderful girlfriend, Aniek van Kersen, for being there by me throughout this entire journey.

*Hani Abu-Jurji
Delft, September 2022*

Contents

Nomenclature	vi
1 Introduction	1
1.1 Background	1
1.2 Research Goal	2
1.3 Report Outline	2
2 Scientific Paper	3
3 Literature Review	19
3.1 Introduction	21
3.1.1 Brief Overview of Non-Destructive Testing	21
3.1.2 Recent Applications of Aerial Manipulators	21
3.1.3 Research Question	22
3.1.4 Literature Review Outline	22
3.2 Aerial Manipulation	24
3.2.1 Rigid Tools	24
3.2.2 Active Robotic Manipulators	25
3.3 Centralized vs. Decentralized Control	27
3.3.1 Centralized Control	27
3.3.2 Decentralized Control	27
3.4 Control Methods	29
3.4.1 Manipulator Control	29
3.4.2 Vehicle Control	32
3.5 Force Estimation	34
3.5.1 Momentum-Based External Force Estimator	34
3.5.2 Kalman Filtering	34
3.5.3 Other Methods	35
3.6 Research Opportunity	36
3.7 Conclusion	38
References	39

Nomenclature

Abbreviations

Abbreviation	Definition
CoM	Centre of Mass
DoF	Degree of Freedom
NDT	Non-Destructive Testing
UAV	Unmanned Aerial Vehicle

Symbols

Symbol	Definition	Unit
C	Manipulator Coriolis & centripetal torque matrix	$[\text{kg} \cdot \text{m}^2 / \text{s}]$
D	Damping matrix	$[\text{kg}/\text{s}]$
F	Force vector	$[\text{N}]$
g	Gravitational acceleration	$[\text{m}/\text{s}^2]$
G	Manipulator gravity torque vector	$[\text{N} \cdot \text{m}]$
h	Wrench vector	$[\text{N} ; \text{N} \cdot \text{m}]$
i	Current	$[\text{A}]$
I	Moment of inertia	$[\text{kg} \cdot \text{m}^2]$
J	Jacobian matrix	$[\text{m}]$
K	Stiffness matrix	$[\text{N}/\text{m}]$
K_τ	Motor torque constant	$[\text{N} \cdot \text{m} / \text{A}]$
l	Link length	$[\text{m}]$
L	Lagrangian	$[\text{J}]$
m	Mass	$[\text{kg}]$
M	Manipulator inertia matrix	$[\text{kg} \cdot \text{m}^2]$
p	Generalized momentum	$[\text{kg} \cdot \text{m} / \text{s}]$
P	Power	$[\text{W}]$
q	Joint angle	$[\text{rad}]$
T	Kinetic energy	$[\text{J}]$
v	Cartesian velocity vector	$[\text{m}/\text{s}]$
V	Potential energy	$[\text{J}]$
W	Work	$[\text{J}]$
x	Cartesian position vector	$[\text{m}]$
α	End-effector angle from centre-line	$[\text{rad}]$
ϵ	Minimization cost function	$[-]$
θ	Pitch angle	$[\text{deg}]$
κ	Condition number	$[-]$
τ	Torque	$[\text{N} \cdot \text{m}]$
ϕ	Roll angle	$[\text{deg}]$
ψ	Yaw angle	$[\text{deg}]$

1

Introduction

1.1. Background

Unmanned aerial vehicles (UAVs) have become increasingly more prevalent in society over recent years as they provide the ability to take to the skies without the need of a human pilot. Since the first quadrotor, many advancements have been made to make these UAVs stronger, faster, and more agile, thus making them potentially more useful in commercial and industrial markets. Despite their rapid development, most modern UAVs are typically designed for traditional applications such as visual surveillance. Until more recently, UAVs have rarely been made to interact with their surrounding environments, thus limiting their potential.

A new line of development has begun to pave the way for a subset of UAVs, named *aerial manipulators* which are designed and controlled specifically for the purpose of robotically interacting with objects and surfaces. These aerial manipulators employ actuators, such as grippers or robotic arms, that work in conjunction with the vehicle to perform specific tasks while in flight. They can prove to be quite useful, especially for some industrial interaction tasks, such as autonomous drilling, hammering, and sensor placement. One more field which is of particular interest is that of non-destructive testing (NDT). The purpose of NDT is to perform routine analysis and evaluation of structures and materials without deforming or causing damage to the piece being examined. This process is critical for ensuring the integrity of various structures. These inspections are typically done by human operators which is not always an easy feat, especially when the structure is difficult to reach, such as a wind turbine blade. By sending in aerial manipulators, rather than human operators, these critical tasks can then be completed autonomously, thus ensuring the safety of the structure as well as the workers can be better assured.

Various designs of these aerial manipulators have been presented throughout different research contributions, some even delving specifically into the field of NDT. For example, Bodie et al. demonstrated the potential for aerial inspections by proposing an aerial manipulator composed of a tilt-rotor UAV for tracing the contours of arches [1]. Trujillo et al. developed a similar aerial manipulator equipped with an ultrasonic sensor for the specific purpose of performing aerial inspections of oil & gas pipes [2]. In both cases, the systems are capable of interacting with complex, curved structures, however they rely heavily upon complex flight controllers and tilt-rotor configurations.

In contrast to these two examples, Hamaza & Kovac propose an alternative approach to aerial interactions [3]. In their work, they present the concept of a quadrotor equipped with a parallel manipulator which is capable of rotating about the vehicle's body. This concept named Omni-Drone is the inspiration for this thesis. The following expands on the work by Hamaza & Kovac by developing the Omni-Drone system and implementing an interaction controller so as to demonstrate its potential for performing contact-based inspection tasks.



Figure 1.1: Example scenario of the Omni-Drone concept demonstrating the potential for NDT inspections of pipe walls. Image source: Hamaza & Kovac [3]. *Background photo credit: noomcpk/Shutterstock.com*

1.2. Research Goal

The thesis presented herein aims to demonstrate how well an omni-directional aerial manipulator can employ a decentralized control architecture to trace unknown curved surfaces while tracking desired forces through the end-effector. To answer this, we must answer the following sub-questions:

1. How accurately can the applied force at the end-effector be estimated using only the torque feedback of the manipulator's servo motors.
 - (a) What is the mean error in the estimate during the duration of the experiment?
 - (b) How quickly does the force estimator converge after a sudden change in the applied force?
2. How well can the manipulator trace an unknown curved surface while implementing an impedance controller in flight?
3. How accurately can the drone platform maintain its pose when disturbed by the manipulator?
 - (a) What deviations from position and attitude are incurred when the manipulator is rotated about the drone body?
 - (b) What deviations from position and attitude are incurred when the manipulator traces along the unknown curved surfaces?

1.3. Report Outline

This thesis is divided into three primary chapters. The first chapter presented here has gone over background information regarding aerial manipulators and their interactions with environment surfaces. It has also presented the research goal along with the relevant sub-questions. Chapter 2 will present a scientific paper regarding the omni-drone aerial manipulator to answer the research questions. Finally, Chapter 3 will delve into the literature review covering the various applications of aerial manipulators. In doing so, it will also cover the methodologies used in the literature for manipulator force estimation and impedance control. As is discussed in the literature review, the methods have each been researched individually in specific use cases, such as on conventional robotic manipulators, and a gap has been identified which shows the potential to integrate force estimation with impedance control on the omni-drone.

2

Scientific Paper

Sensorless Impedance Control for Curved Surface Inspections Using the Omni-Drone Aerial Manipulator

Abstract—In this work, we develop a novel aerial manipulator system with an omni-directional workspace. The system comprises of a quadrotor platform equipped with a rotating five-bar linkage, and serves the purpose of contour tracing tasks on complex shapes, whilst airborne. In order to remove the dependency on additional force sensors and keep the design lightweight, onboard force estimation is implemented based on the generalized momentum of the system, using the torque feedback from the manipulator’s actuators. The computed force estimate feeds in a position-based impedance controller with the purpose of maintaining continuous contact through the manipulator’s end-effector as the system traces contours of unknown curved geometry. Results demonstrate the estimator’s ability to track the applied forces, while the impedance controller shows adequate contour following capabilities. The preliminary results obtained on both stationary and flight experiments validate this approach and show potential for aerial contact inspections of more complex structures.

I. INTRODUCTION

Robotic manipulation is widely used across various industries to automated interaction tasks which could often be too laborious, tedious or hazardous for humans. Various control methodologies have been developed over the years to perform these tasks, but the systems that on which they have been implemented are typically rigidly fixed to the ground. Recent advancements in drone technology have made it possible to develop *aerial manipulators* which are unmanned aerial vehicles (UAVs) capable of physically interacting with the environment [1]. This is typically achieved through the integration of specific tools on the vehicle’s body that allow it to autonomously perform tasks such as scanning, grasping, and transportation of other objects. One of the most promising use cases for these aerial manipulators is the contact-based inspection of industrial areas, especially when dealing with high-rise or difficult-to-reach structures.

A particular field of contact-based inspections is referred to as non-destructive testing (NDT). As described by Gholizadeh, NDT involves the analysis of existing structures and components without causing damage or permanent change to the piece [2]. These inspections normally involve sensors that are capable of obtaining eddy current, magnetic, or electromagnetic measurements and thus the corresponding sensor must be kept consistently in good contact with the inspected material surface in order to ensure that the obtained data is reliable. For this to be done using aerial systems, consistent contact needs to be achieved without disrupting or destabilizing the flight control.

Various designs of these aerial manipulators have been proposed throughout the literature as their potential becomes

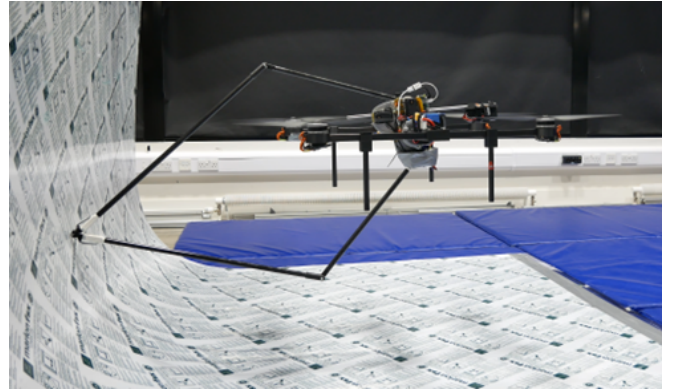


Fig. 1: Omni-Drone in flight

more apparent. Works by Hamaza et al. [3] and Meng et al. [4] show aerial systems capable of performing surface interactions while traversing tangentially with the surface. Aerial NDT inspections have been accomplished by Zang et al. [5]. The system is autonomously guided toward a 2D aluminum sample and takes measurements while maintaining contact. To do this, the UAV follows a predefined trajectory based on accurate knowledge of the vehicle’s and target surface’s respective positions. This would not be ideal in a true setting as it would require a full accurate model of every structure that is to be inspected by the system.

Advancements have been made to this end by Nguyen and Lee where they present the design of a quadrotor with a static tool attached either to the top or the bottom of the vehicle [6]. By relating the vehicle’s dynamics to the tool’s end-effector frame, the flight controller becomes capable of driving the tool’s position to desired locations along the environment while maintaining desired forces. The issue that arises with this is that quadrotors are inherently under-actuated, and thus its operational space is drastically limited, especially in the pitch and roll directions. Improving upon this, work by Bodie et al., has pursued research into three dimensional interactions in two complementing works [7], [8]. In both cases, a fully-actuated UAV is fitted with a rigid boom for interactions with 3D contours. Similarly, Trujillo et al. developed an eight tilted-rotor UAV with an active robotic manipulator for the specific purpose of performing NDT in the Oil & Gas industry [9].

The addition of active robotic arms with varying Degrees of Freedom (DoFs) has also been explored and reduce the extent of the motion required by the UAV to reach different workspaces [10]. A single-DoF linear manipulator mounted to the top of a UAV has been developed by Hamaza et al. [3] to

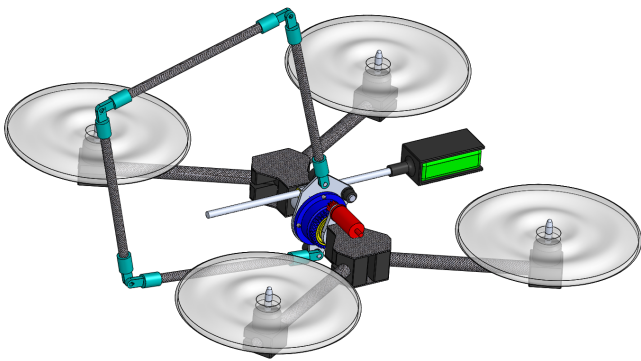


Fig. 2: CAD drawing of Omni-Drone concept from work by Hamaza & Kovac [11]. Figure includes five-bar linkage with rotating flange along with counter-balance.

exert forces of known value and profile to front-facing targets without relying on the UAV's flight controller to compensate for disturbances, but rather using the active manipulator to achieve robust and stable interaction.

So far, aerial manipulation systems have for the most part been designed to aid with tasks executed either below or to the side of the UAV. A design that widens the reachable workspace of the system and thus makes it more versatile was formerly introduced by Hamaza and Kovac [11]. In the work, the design was conceptualized to perform contact-based inspection tasks of tunnels, caves, and other complex geometries and it serves as the basis of the design of the aerial manipulator used in the following research. It consists of a conventional quad-rotor equipped with an active five-bar manipulator attached to the vehicle's centre of mass capable of pivoting about the vehicle and offering an omni-directional workspace. Radial extension and retraction is attained through the actuation of the two base joints of the manipulator. Planar azimuthal motion is done by pivoting the entire manipulator linkage around the vehicle body. The final out-of-plane motion is then lastly achieved through the yaw-motion of the UAV. A CAD drawing of the concept is presented in Figure 2.

In this paper we present further design and kinematics development along with the implementation of a control strategy based on onboard force estimation for a sensorless impedance controller to perform contour following tasks along a curved surface. The goal is to demonstrate the capability of the novel aerial manipulator, with omni-directional reachability. We wish to demonstrate that a position-based impedance controller can be implemented without the need for additional force sensors, but rather by using an estimation scheme based purely on the torque feedback of the motors. By showing adequate contour tracing, it would be possible to extend this work to curved surface-based inspection tasks.

The outline of this paper will be as follows. Firstly, we delve into related works regarding control architectures, interaction control, and force estimation of robotic manipulators. Secondly, the system description is discussed, looking into the manipulator and vehicle subsystems of the Omni-Drone. Following this, the mathematical model of the system defining both the kinematics and dynamics is derived. This leads to

the development the control architecture, consisting of the force estimator and impedance controller. This then leads to a presentation of the results of both the validation of the force estimator followed by the results of the force tracking task in flight. Finally, we will present an outlook to future works.

II. RELATED LITERATURE

We intend to employ the Omni-Drone aerial manipulator to perform contour tracing tasks of curved surfaces without the need for additional force/torque sensors. To do so, we must consider three key aspects of the aerial manipulator:

- Control architecture
- Interaction controller
- Force estimation

The following section reviews various publications regarding each of these topics. We draw from the methods presented in the literature to develop the the Omni-Drone for its intended task.

A. Control Architecture

It is possible to develop control architectures where the control of the end-effector is done through coordination of both the flight control and the manipulator control. This concept is referred to as *centralized control* as seen in the works of Kim et al. [12] and by Heredia et al. [13]. In these cases a single integrated controller addresses both the flight states (attitude, position, velocity) as well as the manipulator states (joint angles, velocities, torques). Alternatively, a *decentralized control* method treats the aerial platform and the manipulator as two separate entities. Works by Tognon et al. [14] and Thomas et al. [15] use this method on systems comprised of a quadrotor and 2-DoF manipulator, where the position and torque control of the manipulator remains completely independent of the attitude and position control of the vehicle. By separating the manipulator control from the flight control, the aerial vehicle could be designed to simply hover near a target and allow the manipulator to work independently. The aerial vehicle would then effectively treat the resulting effects of the manipulator as external disturbances.

B. Interaction Control Methods

When performing contact-related tasks with unknown environments, inherently imposed constraints must be supervised. As explained by Villani and De Schutter [16], pure motion control in these situations may lead to potential damage of the manipulator and/or the environment. Therefore, the manipulator control in these constrained environments must account for a level of *compliance*, in either passive and/or active manners. Some passive methods could employ the use of spring elements such as in the work by Bartelds et al. [17] where mechanical compliance is achieved by means of an elastic band. In contrast, active compliance methodologies achieve their purpose through programmed control systems, which afford the ability to tune the behaviour and achieve more suitable compliance.

A popular method of active compliant control is through *impedance control* where the end-effector's deviation from a defined desired motion is directly related to the experienced contact wrench with the environment [16]. This relationship is defined by a virtual mechanical impedance of the system and is obtained by modelling the system as a mass-spring-damper. Suarez et al. [18] have used this methodology to perform the control of a dual-arm aerial manipulator for pipe inspections. Extensions of the classical impedance controller have also been developed, mainly on industrial robots, where the impedance parameters of the controller are dynamically adjusted such as in the works by Car et al. [19] and Marković et al. [20]. In the latter paper, the authors develop an adaptation law which is dependent on the force error, its derivative, and an additional auxiliary parameter. Simpler works, which are less susceptible to noise have been accomplished by the likes of Lee and Buss [21], Lu et al. [22], and finally by Roveda and Piga [23], where both the stiffness and damping parameters of the control system are increasingly adapted as the force error tends to zero. This idea of an adaptive impedance controller has also been implemented on an underwater vehicle with robotic arm in the work of Cieślak and Ridao [24].

C. Force Estimation

Knowledge of the applied force is critical when implementing impedance control and research involving manipulators typically employ sensors to measure the contact wrench. For example, a UAV with a bottom-mounted robotic arm designed by Buzzatto et al. [25] relies on a six-axis force/torque sensor which feeds the measurements directly to the vehicle's controller. The issue with this approach is that these sensors may physically interfere with other equipment, such as NDT sensors. They also introduce additional weight and costs to the system.

Rather than directly measuring these forces, one could also estimate them from other observable states. Ruggiero et al. [1] utilize the generalized momentum, derived from the linear and angular momenta of the system. With this, a linear relationship can be derived to construct an external observer for estimating the wrench. This method has been implemented within two different contributions by Bodie et al. [7], [8] where the external wrench estimator yields estimates of the forces and torques experienced at the end-effector using only measurements of the linear and angular velocities.

An alternative approach presented by Roveda and Piga [23] where they have implemented a sensorless Extended Kalman Filter (EKF) [26] to estimate the contact force of the manipulator's end-effector. A similar implementation has also been seen in the work by Fakoorian et al. [27] where they estimate the ground reaction forces of prosthetic legs. It is possible to combine the concept of generalized momentum from above with the Kalman filter approach to develop a linear estimator for the external force. This method has been presented by Wahrburg et al. [28] where the force vector applied at the end-effector of a serial, industrial manipulator is estimated using the generalized momenta of the joints. The benefit of this method, is that the system of equations defining

the dynamics of the manipulator may be set up in such a way that a linear Kalman filter could be employed. This greatly simplifies the algorithm and guarantees optimality of the estimation.

III. SYSTEM

The aerial manipulator system is composed of two distinct subsystems which act independently to perform the interaction tasks. They are described as follows.

A. Manipulator

The robotic manipulator is designed as a parallel five-bar linkage consisting of carbon fibre tubes for the four main links and an aluminum flange that makes up the fifth, base link. This flange includes a ball bearing sleeve with a 50mm inner diameter that affords the ability to rotate entirely around the drone body. This rotation is driven by a spur gear interface where the exterior of the bearing housing acts as the driven gear. Mounted on the flange itself are three Dynamixel MX-64A servo motors. Two of these motors actuate the active joints of the five-bar linkage while the third drives a rack and pinion counter-balance. For clarity throughout this paper, we will refer to the two motors for the active joints as *Motor 1* and *Motor 2*, while the rack and pinion motor will be referred to as *Motor 3*.

B. Platform

The aerial platform is a conventional H-configuration quadrotor equipped with T-Motor MN501-S KV360 motors and 18-inch propellers. The onboard flight controller is a Pixhawk PX4 providing PID control of the drone in position mode. Also mounted to the frame of the quadrotor is a Dynamixel XM-540WR servo motor equipped with a spur gear. This gear interfaces with the manipulator's rotating flange to give the system its pivoting capability.

IV. MODELLING

A. Reference Frames

The modelling and control of the Omni-Drone system utilizes several different frames of reference. This brief subsection will provide an overview of each of these frames and describe their importance for the work presented in this paper.

1) *World Frame*: The world frame will be defined as the static frame of reference in which we will define the position, velocity, and acceleration of the UAV. Its origin will be fixed, with the Z axis pointing upward from the ground and the X and Y axes being set arbitrarily such that X , Y , and Z are orthogonal. This frame may be perceived as inertial as it will only consider the local environment of the UAV.

2) *UAV Body Frame*: The UAV body frame will be used to define the kinematics and dynamics of the quadrotor itself. For this, the origin of the frame is fixed at the centre of mass of the UAV. The X axis points directly forward through the centre-line of the UAV, the Y axis points to the left, and the Z axis initially points directly upward, taken from when the UAV is in a steady, stable hover.

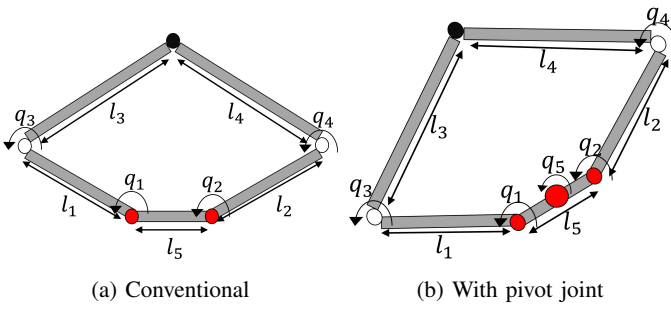


Fig. 3: Depiction of both the five bar parallel linkage and the five-bar parallel linkage with pivot joint with relevant parameters.

3) *Manipulator Body Frame*: The manipulator body frame will be useful in defining the kinematics and dynamics of the manipulator. It is defined by having the origin fixed at the manipulator's pivot joint where the X axis points to the right, the Y axis points up, and the Z axis points outward. In this frame, the rotation angle of the manipulator is not considered. To transform from the manipulator body frame to the UAV body frame, a single-axis rotation is applied equal to the pivot angle q_5 .

B. Parameters

In order to model our system, we must first present the parameters and variables which will define the configuration of the manipulator. Figure 3 depicts schematics of both a conventional five-bar parallel linkage (left) and the one proposed with the active pivot joint included (right). There are a total of three active joints. The first two, defined as q_1 and q_2 , connect the left and right legs of the manipulator to the rotating flange. The third is the pivot joint, q_5 , about which the whole manipulator rotates around the UAV body. There are two passive joints, q_3 and q_4 , that hinge the two segments together in each leg. As passive joints, they are not directly controlled by actuators, however their angles and angular velocities can be computed directly from joints q_1 and q_2 .

C. Manipulator Kinematics

When dealing with interaction tasks, our primary concern is in the motion of the end-effector of the parallel manipulator. In other words, we are concerned in the polar coordinate representation of the end-effector's position and velocity with respect to the UAV's centre of mass. Though the point of interest is the end-effector, the control of the manipulator is driven through the two active joints at the base of the five-bar linkage, namely Motor 1 and Motor 2. Thus, this introduces two key coordinate spaces when controlling and observing the manipulator. These spaces are the *Joint Space*, defining the angular positions, velocities and accelerations of the joints, and the *Task Space*, defining the Cartesian/polar representation of the position, velocity and acceleration of the end-effector. The transformation from the joint space to the task space is defined as the *Forward Kinematics*, while the transformation

from the task space to the joint space is defined as the inverse kinematics. These two transformations will subsequently be derived for the five-bar parallel linkage, both of which will be required to perform the control and sensing tasks of the aerial interaction.

1) *Forward Kinematics*: The purpose of the forward kinematics is to derive the position and velocity of the end-effector from knowledge of the angular positions and velocities of the manipulator's active joints. We treat the manipulator as a conventional, non-rotating five-bar parallel linkage. Noting the dependent relationships between the four joints. These constraints can be expressed through the following equations:

$$\begin{aligned} \frac{-l_5}{2} + l_1 \cos q_1 + l_3 \cos q_3 &= \frac{l_5}{2} + l_2 \cos q_2 + l_4 \cos q_4 \\ l_1 \sin q_1 + l_3 \sin q_3 &= l_2 \sin q_2 + l_4 \sin q_4 \end{aligned} \quad (1)$$

Equations (1) denote the geometric relationships for the x and y end-effector coordinates respectively by equating the left and right halves of the manipulator. We can rearrange equations (1) to define $x_1 = l_1 \cos q_1 + l_3 \cos q_3$ and $x_2 = l_5 + l_2 \cos q_2 + l_4 \cos q_4$. The joint angles q_3 and q_4 can then be obtained as follows:

$$\begin{aligned} num &= 2l_3x_2 \pm \sqrt{\begin{aligned} &-l_3^4 + 2l_3^2l_4^2 + 2l_3^2x_1^2 + 2l_3^2x_2^2 \\ &-l_4^4 + 2l_4^2x_1^2 + 2l_4^2x_2^2 - x_1^4 - \\ &2x_1^2x_2^2 - x_2^4 \end{aligned}} \\ den &= l_3^2 + 2l_3x_1 - l_4^2 + x_1^2 + x_2^2 \\ q_3 &= 2 \tan^{-1} \frac{num}{den} \end{aligned} \quad (2)$$

$$\begin{aligned} num &= 2l_4x_2 \pm \sqrt{\begin{aligned} &(-l_3^2 + 2l_3^2l_4^2 - l_4^4 + x_1^2 + x_2^2)(l_3^2 \\ &+ 2l_3l_4 + l_4^2 - x_1^2 - x_2^2) \end{aligned}} \\ den &= -l_3^2 - 2l_3x_1 + l_4^2 + x_1^2 + x_2^2 \\ q_4 &= -2 \tan^{-1} \frac{num}{den} \end{aligned} \quad (3)$$

The angular velocities \dot{q}_3 and \dot{q}_4 can be computed from the time derivatives equations (1), written in matrix form:

$$\begin{bmatrix} y_1 \\ y_2 \end{bmatrix} = \begin{bmatrix} a & b \\ c & d \end{bmatrix} \begin{bmatrix} \dot{q}_3 \\ \dot{q}_4 \end{bmatrix} \quad (4)$$

where $y_1 = -l_1\dot{q}_1 \sin q_1 + l_2\dot{q}_2 \sin q_2$, $y_2 = -l_1\dot{q}_1 \cos q_1 + l_2\dot{q}_2 \cos q_2$, $a = l_3 \sin q_3$, $b = -l_4 \sin q_4$, $c = l_3 \cos q_3$, and $d = -l_4 \cos q_4$.

These results can then easily be substituted into either side of equations (1) to obtain the position and velocity of the end-effector.

2) *Inverse Kinematics*: Contrary to the forward kinematics, the inverse kinematics define the joint angular positions and velocities in terms of the end-effector position and velocity. This will prove to be a useful result as it makes it possible to command the motors to control the end-effector. The procedure for deriving the inverse kinematics of the rotating five-bar parallel linkage has been presented by Hamaza & Kovac [11], briefly reviewed here.

Given a desired end-effector position $\chi = [x_{ee} \ y_{ee}]^T$, the angle which this position makes with respect to the centre-line of the manipulator's pivot point can be computed as:

$$\alpha = \tan^{-1} \left(\frac{y_{ee}}{x_{ee}} \right) \quad (5)$$

Let A and B denote the Cartesian positions of joints 1 and 2 respectively, then we can get:

$$A = \begin{bmatrix} \frac{l_5}{2} \cos \left(\alpha + \frac{\pi}{2} \right) \\ \frac{l_5}{2} \sin \left(\alpha + \frac{\pi}{2} \right) \end{bmatrix} \quad (6a)$$

$$B = \begin{bmatrix} \frac{l_5}{2} \cos \left(\alpha + \frac{3\pi}{2} \right) \\ \frac{l_5}{2} \sin \left(\alpha + \frac{3\pi}{2} \right) \end{bmatrix} \quad (6b)$$

With A and B known, we can then compute the positions of joints 3 and 4. We denote these positions as M_1 and M_2 respectively, which can each be solved for independently, given an end-effector position and knowledge of A and B from above. The position of M_1 can be computed as the intersection of two circles, one centred at A and the other at the end-effector, with radii l_1 and l_3 respectively. The position of M_2 can similarly be computed using point B instead of A . This computation will result in two distinct points of circle-circle intersection for each side of the manipulator. The correct intersection points must be selected, which can be selected as the two points that maximize the distance between them. To visualize, Figure 4 demonstrates the circle-circle intersection with all four intersection points shown. The two points coloured green are selected as they make up the symmetric configuration with the maximum distance between them. Trigonometric relationships can then be used to easily determine the desired joint angles, q_1 and q_2 , as follows:

$$q_1 = \tan^{-1} \left(\frac{M_{1y} - A_y}{M_{1x} - A_x} \right) \quad (7a)$$

$$q_2 = \tan^{-1} \left(\frac{M_{2y} - B_y}{M_{2x} - B_x} \right) \quad (7b)$$

With these results, we are left with the task of computing the pivot angle of the manipulator. It is important to note that its computation is dependent on the roll angle of the UAV as the difference of the pivot angle and the roll angle yield the angular position of the end-effector with respect to the inertial frame. Taking the local horizon as reference, the pivot angle can be computed as:

$$q_3 = \alpha - \phi - \frac{\pi}{2} \quad (8)$$

D. Jacobian Matrix

One important attribute of the system is the Jacobian matrix which relates the system velocities between the task and joint spaces. To derive the Jacobian matrix of the Omni-Drone's manipulator, we first split the linkage into a right-half and a left-half. The x- and y-coordinates of the end-effector can then be expressed using the left hand sides and right hand sides of equations (1) respectively. In brief, this yields the following four equations:

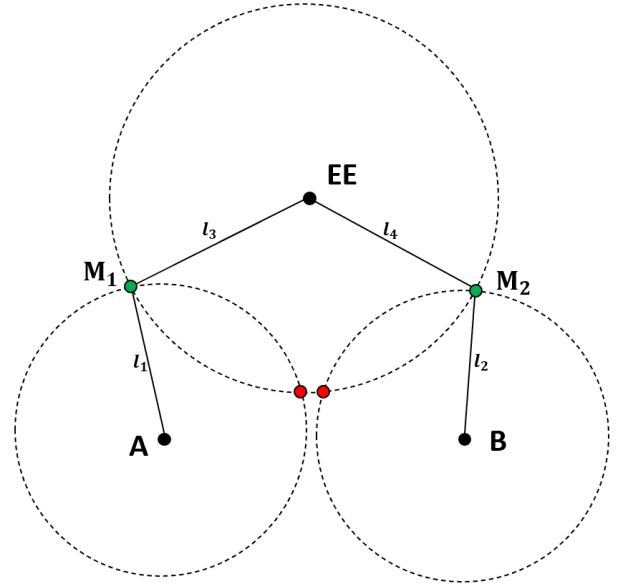


Fig. 4: Circle intersection points to determine points M_1 and M_2 . The green intersection points are selected.

$$\begin{aligned} x_{LHS} &= \frac{-l_5}{2} + l_1 \cos q_1 + l_3 \cos q_3 \\ y_{LHS} &= l_1 \sin q_1 + l_3 \sin q_3 \\ x_{RHS} &= \frac{l_5}{2} + l_2 \cos q_2 + l_4 \cos q_4 \\ y_{RHS} &= l_2 \sin q_2 + l_4 \sin q_4 \end{aligned} \quad (9)$$

The time derivatives of the equations above can easily be taken to express the Cartesian velocity of the end-effector in terms of the angular velocities of the four manipulator joints. This is expressed as:

$$\begin{aligned} \dot{x}_{LHS} &= -l_1 \sin q_1 \dot{q}_1 - l_3 \sin q_3 \dot{q}_3 \\ \dot{y}_{LHS} &= l_1 \cos q_1 \dot{q}_1 + l_3 \cos q_3 \dot{q}_3 \\ \dot{x}_{RHS} &= -l_2 \sin q_2 \dot{q}_2 - l_4 \sin q_4 \dot{q}_4 \\ \dot{y}_{RHS} &= l_2 \cos q_2 \dot{q}_2 + l_4 \cos q_4 \dot{q}_4 \end{aligned} \quad (10)$$

Transcribing the above to linear systems of equations and remembering that the left and right hand sides must always be equal due to the geometric constraint, we get the following:

$$\begin{aligned} \begin{bmatrix} \dot{x} \\ \dot{y} \end{bmatrix} &= \begin{bmatrix} -l_1 \sin q_1 & -l_3 \sin q_3 \\ l_1 \cos q_1 & l_3 \cos q_3 \end{bmatrix} \begin{bmatrix} \dot{q}_1 \\ \dot{q}_3 \end{bmatrix} = \mathbf{J}_1(\mathbf{q}) \begin{bmatrix} \dot{q}_1 \\ \dot{q}_3 \end{bmatrix} \\ \begin{bmatrix} \dot{x} \\ \dot{y} \end{bmatrix} &= \begin{bmatrix} -l_2 \sin q_2 & -l_4 \sin q_4 \\ l_2 \cos q_2 & l_4 \cos q_4 \end{bmatrix} \begin{bmatrix} \dot{q}_2 \\ \dot{q}_4 \end{bmatrix} = \mathbf{J}_2(\mathbf{q}) \begin{bmatrix} \dot{q}_2 \\ \dot{q}_4 \end{bmatrix} \end{aligned} \quad (11)$$

The Jacobian matrix allows us to determine the end-effector velocity from the known joint angular velocities..

The Jacobian can also be used to relate the forces at the end-effector to the torques experienced at the manipulator joints. This will prove to be an important result as it means that the interaction force of the manipulator can be known directly from the torques measured at the actuating motors. We can use the principle of virtual work to derive this relationship.

First we note the definitions of work (W) and power measured at the end-effector (P_{EE}) with respect to the force and velocity of the end-effector in the task space:

$$W = \int \mathbf{F}^T \dot{\mathbf{x}} dt = \mathbf{F}^T \mathbf{x} \quad (12)$$

$$P_{EE} = \frac{W}{t} = \frac{\mathbf{F}^T \mathbf{d}}{t} = \mathbf{F}^T \dot{\mathbf{x}} \quad (13)$$

In parallel, we can also define the power of each motor as the product of their torques and angular velocities:

$$P_{joint} = \boldsymbol{\tau}^T \dot{\mathbf{q}} \quad (14)$$

The conservation of power at the end-effector equates to the power at the joints, yielding:

$$\begin{aligned} P_{EE} &= P_{joint} \\ \mathbf{F}^T \dot{\mathbf{x}} &= \boldsymbol{\tau}^T \dot{\mathbf{q}} \\ \mathbf{F}^T \mathbf{J}(\mathbf{q}) \dot{\mathbf{q}} &= \boldsymbol{\tau}^T \dot{\mathbf{q}} \end{aligned} \quad (15)$$

Rearranging the result from above yields the representation of the force at the end-effector with respect to the torques of the joints:

$$\mathbf{F} = \mathbf{J}^{-T}(\mathbf{q}) \boldsymbol{\tau} \quad (16)$$

Using this general relationship, it is important to recall that we previously defined the Jacobian for the left and right hand sides of the manipulator independently. The total force experienced at the end-effector is thus the sum of the two individual transformations (i.e. $\mathbf{F}_{total} = \mathbf{F}_{LHS} + \mathbf{F}_{RHS}$). We also note that the torques of the passive joints (i.e. joints 3 and 4) are zero; thus the columns corresponding to these joints may be omitted. Summing the relationships for the two legs of the manipulator gives the following definition of the total force with respect to the joint torques:

$$\mathbf{F} = \begin{bmatrix} -l_1 \sin q_1 & -l_2 \sin q_2 \\ l_1 \cos q_1 & l_2 \cos q_2 \end{bmatrix} \begin{bmatrix} \tau_1 \\ \tau_2 \end{bmatrix} \quad (17)$$

E. Manipulator Dynamics

In order to model the manipulator's dynamics, system's equations of motion need to be derived. For any generic manipulator, the motion is described as:

$$\mathbf{M}(\mathbf{q}) \ddot{\mathbf{q}} + \mathbf{C}(\mathbf{q}, \dot{\mathbf{q}}) \dot{\mathbf{q}} + \mathbf{G}(\mathbf{q}) = \boldsymbol{\tau}_m - \boldsymbol{\tau}_{ext} \quad (18)$$

where $\mathbf{M}(\mathbf{q})$ and $\mathbf{C}(\mathbf{q}, \dot{\mathbf{q}})$ denote the system's inertia and Coriolis & Centrifugal matrices. The torque due to gravity is represented by $\mathbf{G}(\mathbf{q})$ while $\boldsymbol{\tau}_m$ denotes the torque at the joints and $\boldsymbol{\tau}_{ext}$ denotes the torques due to external disturbances to the system.

The derivation of these can be done using the Lagrangian formulation:

$$L = T - V \quad (19)$$

where T and V denote the kinetic and potential energies of the system respectively. The equations of motion can then be computed as:

$$\frac{d}{dt} \frac{\partial L}{\partial \dot{\mathbf{q}}} - \frac{\partial L}{\partial \mathbf{q}} = \boldsymbol{\tau}_m - \boldsymbol{\tau}_{ext} \quad (20)$$

The following presents the kinetic and potential energy terms of the system which will subsequently be differentiated in order to apply equation 20.

1) *Kinetic Energy*: We can break down the kinetic energy of the system into the individual components, denoting respective masses and moment of inertia of each link i as m_i and I_i . Since we are only concerned with rotations about the out-of-plane z-axis of the manipulator body frame, the moments of inertia reduce to scalar quantities, I_{zzi} , yielding:

$$T_1 = \frac{1}{2} I_{zzi} \dot{q}_1^2 \quad (21)$$

$$T_2 = \frac{1}{2} I_{zzi} \dot{q}_2^2 \quad (22)$$

To compute the kinetic energies of the links 3 and 4, we first need to compute the position and velocity vectors of their respective centres of mass.

$$\begin{aligned} \mathbf{r}_{c3} &= \begin{bmatrix} l_1 \cos q_1 + l_{c3} \cos q_3 \\ l_1 \sin q_1 + l_{c3} \sin q_3 \end{bmatrix} \\ \mathbf{r}_{c4} &= \begin{bmatrix} l_2 \cos q_2 + l_{c4} \cos q_4 \\ l_2 \sin q_2 + l_{c4} \sin q_4 \end{bmatrix} \\ \mathbf{v}_{c3} &= \begin{bmatrix} -l_1 \sin q_1 \dot{q}_1 - l_{c3} \sin q_3 \dot{q}_3 \\ l_1 \cos q_1 \dot{q}_1 + l_{c3} \cos q_3 \dot{q}_3 \end{bmatrix} \\ \mathbf{v}_{c4} &= \begin{bmatrix} -l_2 \sin q_2 \dot{q}_2 - l_{c4} \sin q_4 \dot{q}_4 \\ l_2 \cos q_2 \dot{q}_2 + l_{c4} \cos q_4 \dot{q}_4 \end{bmatrix} \end{aligned} \quad (23)$$

The kinetic energies of the two links can then be expressed as:

$$T_3 = \frac{1}{2} I_3 \dot{q}_3^2 + \frac{1}{2} m_3 \|\mathbf{v}_{c3}\|^2 \quad (24)$$

$$T_4 = \frac{1}{2} I_4 \dot{q}_4^2 + \frac{1}{2} m_4 \|\mathbf{v}_{c4}\|^2 \quad (25)$$

A similar computation can be made for the end-effector's kinetic and potential energies, however we will compute it using the left and right links of the manipulator and take the average of the two. The reason for this is to ensure that the resulting equations of motion contain contributions from all four joints when describing the dynamics of the end-effector. For this, we use equations (10) to define the end-effector's velocity as $\mathbf{v}_{EE1} = [\dot{x}_1 \ \dot{y}_1]^T$ and $\mathbf{v}_{EE2} = [\dot{x}_2 \ \dot{y}_2]^T$. The kinetic energy can then be expressed as:

$$T_{EE} = \frac{1}{2} m_{EE} \left(\frac{1}{2} \|\mathbf{v}_{EE1}\|^2 + \frac{1}{2} \|\mathbf{v}_{EE2}\|^2 \right) \quad (26)$$

2) *Potential Energy*: The gravitational potential (i.e. $V_g = mgy$, where $g = 9.81 \text{ m/s}^2$ is computed about pivot joint, coinciding with the Centre of Mass (CoM) of the aerial system. The potential energy terms of the four links can then be computed as:

$$\begin{aligned} V_1 &= m_1 g l_{c1} \sin(q_1 + q_5) \\ V_2 &= m_2 g l_{c2} \sin(q_2 + q_5) \\ V_3 &= m_3 g l_{c3} \sin(q_3 + q_5) \\ V_4 &= m_4 g l_{c4} \sin(q_4 + q_5) \end{aligned} \quad (27)$$

In a similar manner to the kinetic energy derivation, the potential energy of the end-effector can be computed by averaging the left and right hand sides of the manipulator:

$$\begin{aligned} V_{EE} &= \frac{1}{2} m_{EE} g (l_1 \sin(q_1 + q_5) + l_3 \sin(q_3 + q_5) \\ &\quad + l_2 \sin(q_2 + q_5) + l_4 \sin(q_4 + q_5)) \end{aligned} \quad (28)$$

To obtain the equations of motion in the form of (18), the results above are substituted into (19). $M(q)$ and $C(q, \dot{q})$ are obtained by arranging the resulting equations based on the terms that pre-multiply \ddot{q} and \dot{q} respectively. The remaining terms make up $G(q)$.

V. TASK SPACE OPTIMIZATION

One of the design decisions required for the robotic manipulator regards the lengths of each of the links that make up the five-bar parallel manipulator. Three variables define the geometry of the manipulator: l_c , l_1 , and l_2 , denoting the lengths of the base, bottom, and top links respectively. The rotating flange imposes a mechanical constraint to the base length l_c and as such, this parameter is defined.

This optimization problem aims to maximize the reachable workspace of the manipulator, which in the case of a five-bar parallel linkage, does not necessarily grow continuously as the lengths of the links increase. As explained by Hamaza and Kovac [11], the workspace of the manipulator is defined as the set of all reachable spatial points for a given geometry. For an arbitrary rotating five-bar linkage geometry, this workspace results in a ring around the pivot point of the manipulator. In addition to simply reaching the space, we must also consider the existence of singularities which result from particular configurations. These singularities are defined when the Jacobian of the system is ill-conditioned, typically due to the passive joints being in a fully-extended position. Lastly, by increasing the extendable reach of the manipulator, we inherently increase the system's moment of inertia, which again is dependent on the configuration. Thus, we end up with an optimization problem where we wish to:

- 1) maximize the area of the workspace
- 2) minimize the number of singularities
- 3) minimize the maximum possible moment of inertia caused by the given geometry

Before performing the optimization, we must first develop the three sub-objective functions which are to be minimized.

A. Reachable Workspace

To maximize the reachable workspace of the manipulator, we can set up a search space around the vehicle's CoM. By solving the inverse kinematics problem, we can derive the set of reachable coordinates in space for a given geometry. In doing so, we also derive the unreachable positions resulting from singularities. Mathematically, we can define this as:

$$\epsilon_1 = \frac{n(\mathcal{S})}{n(\mathcal{A})} \quad (29)$$

where $n(\mathcal{S})$ denotes the quantity of singularities and $n(\mathcal{A})$ denotes the number of points in the search space.

B. Condition Number

It is important to also minimize the ill-conditioned configurations resulting from the geometry. The metric for this is the Jacobian matrix's *condition number*. It is a measure of how much the output of the system will change for a small

given change in the input. We sum over all of the Jacobian condition numbers corresponding to reachable positions. After this, the goal is to find the geometry which minimizes this total condition number. This cost function can be represented as follows:

$$\epsilon_2 = \sum_i \kappa(\mathbf{X}_i) \quad (30)$$

where $\kappa(\mathbf{X}_i)$ denotes the condition number for an end-effector position X_i in the search space.

C. Moment of Inertia

The final contributing factor to be considered is the resulting moment of inertia. The manipulator is expected to induce a large moment arm, which could impact the flight mechanics of the vehicle as well as the actuator driving the pivot motion. It can easily be seen that for any given geometry, there are two possible configurations which are candidates for the maximum moment of inertia: 1) Fully extended (where the end-effector is located far from the CoM of the UAV); and 2) Fully retracted (where the two passive joints of the manipulator are furthest apart). We compute the maximum moment of inertia in these two configurations for each geometry with the intention of minimizing this value. This is done by computing the 2x2 moment of inertia matrices, \mathbf{I}_i , for each of the rod links of the manipulator and apply the parallel axis theorem to obtain the total moment of inertia matrix of the manipulator in a given configuration. We can then take the maximum element from all possible moment of inertia matrices for a given geometry in all configurations:

$$\epsilon_3 = \max(\mathbf{I}_i) \quad (31)$$

Taking these three factors into account, the intention is to minimize the cumulative, weighted objective function, consisting of all three of the above sub-objectives to determine the optimal link lengths $\lambda = [l_c \ l_1 \ l_2]$:

$$\lambda = \arg \min_{\lambda} w_1 \epsilon_1 + w_2 \epsilon_2 + w_3 \epsilon_3 \quad (32)$$

s.t. $l_c = l_{c_{fixed}}$

where w_1 , w_2 , and w_3 denote the weights attributed to each sub-objective and $l_{c_{fixed}}$ represents the mechanical constraint on the base link. Here, an equal weight distribution was given across the three sub-objectives.

We can then formulate a *genetic algorithm (ga)* to minimize the cost function. The algorithm stochastically finds the optimal state by iterating over a population of candidate solutions. It then updates or discards these candidate solutions based on their *fitness* (i.e. the objective function). In short, the algorithm works as follows:

- 1) Initialize population with random candidate solutions.
- 2) Evaluate the objective function for each candidate solution.
- 3) Stochastically discard a portion of the candidate solutions, where the solutions with a worse objective function are more likely to be discarded.
- 4) Select pairs of "parent" candidate solutions and regenerate the population where each "child" retains some solution traits from each "parent".

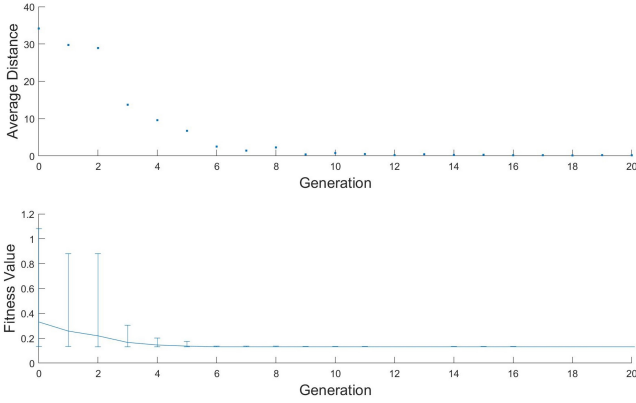


Fig. 5: Results of the genetic algorithm optimiser over 20 generations. First plot depicts the average state-space distance of each population member. Plot two depicts the average, maximum, and minimum cost function evaluation for each generation.

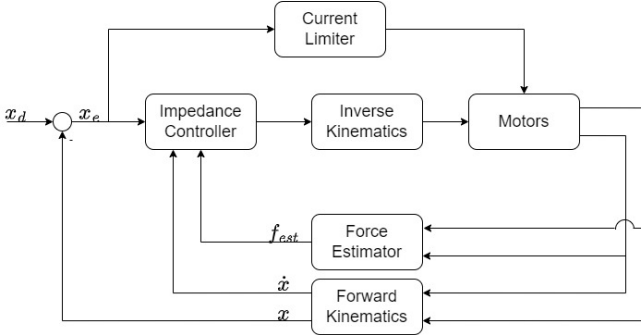


Fig. 6: Control System Block Diagram

5) Repeat from step 2, until a termination condition is met.

The termination condition occurs when either the average fitness function does not significantly change over the course of a few generations, or a maximum time condition is met.

Figure 5 presents the results of the GA optimizer over the course of 20 generations. We can see that after 9 generations, the algorithm converged to its optimum. The optimal geometry is $l_c = 19.76 \text{ cm}$, $l_1 = 47 \text{ cm}$ and $l_2 = 71.5 \text{ cm}$.

VI. CONTROL ARCHITECTURE

A. Counter-Balance Control

One of the three motors on the manipulator's flange is used to drive a rack and pinion counter-balance. Effectively, the counter-balance is driven to a distance from the pivot point such that the new moment around the pivot point remains zero at all times. This can simply be done by first finding the resulting moment induced by the manipulator at a given configuration. To do this, the positions of the centres of mass of each link, as well as the end-effector, are first computed from the joint angles q_1 and q_2 through forward kinematics. Denoting the masses of the four links and the end effector as

m_1, m_2, m_3, m_4 and m_{EE} , then the total moment induced by the manipulator can be computed as:

$$M_{total} = m_1 y_{c1} + m_2 y_{c2} + m_3 y_{c3} + m_4 y_{c4} + m_{EE} y_{EE} \quad (33)$$

where y_{ci} denotes the y-distance in the body frame of the cCoM of link i and y_{EE} denotes the y-distance in the body frame of the end-effector. Note that due to the symmetry of the manipulator, only the moment in the y-direction needs to be offset.

We can now compute the required distance for the counter-balance, however one must take care as counterbalance mechanism itself increasingly contributes to the counter-moment as it protrudes out. The moment induced by the counter-balance:

$$M_{CB} = m_{mass} y_{mass} + \rho_{rack} \pi r_{rack}^2 y_{rack}^2 \quad (34)$$

where m_{mass} and l_{rack} denote the mass and y-distance of the CoM of the counter-weight respectively. The parameters ρ_{rack} , r_{rack} and y_{rack} each denote the density, radius, and y-distance of the aluminum rack respectively. The CoM of the counter-weight does not sit directly at the end of the rack, but rather at a distance d from the end. Thus we can express the distance of this counter-weight as $y_{mass} = y_{rack} - d$. Substituting (34) yields:

$$M_{CB} = \rho_{rack} \pi r_{rack}^2 y_{rack}^2 + m_{mass} y_{rack} - m_{mass} d \quad (35)$$

Equation (35) is quadratic in terms of y_{rack} , and thus can be solved to determine the position for the extension of the counter-balance rack. In summary, the total moment of the manipulator system is nullified by continuously reading the values of q_1 and q_2 , computing the induced manipulator moment through forward kinematics, computing the required extension of the counter-balance rack. This extension can easily be converted to a motor command through the arc length equation, noting the pitch circle diameter (PCD) of the gear.

B. Current Limit Control

Motor 1 and Motor 2 of the parallel manipulator are set to the current-based position control mode. The reason for this is to provide a level of compliance by greatly limiting the current while the motor positions are near the desired positions. Simply using the PD control of the motors in position control mode leads to one of two scenarios: either the gains are too low such that the motors are unable to reach the desired position goal due to external torques such as gravity acting on the manipulator, or the gains are so large that the motors are too stiff and that loads at the end-effector of the manipulator induce enormous current draws to maintain the position. Due to this, the current-based position control mode is used to provide mechanical compliance and protect the motors and other electronics from current wind-up. An additional proportional controller is implemented to current commands to the current-based position controller. The open loop control law of this method can simply be expressed as:

$$i_c = i_{init} + P_i(q_d - q) \quad (36)$$

where i_{init} is a nominal current value which is commanded at zero position error, q_d and q are the desired and measured angular positions. In this manner, the parallel linkage

behaves with linearly increasing stiffness as the position error increases.

C. External Force Estimator

As previously mentioned, we can directly relate forces applied at the end-effector to the resulting torques at the motors through the Jacobian of the system. In theory, this means that the force applied at the end-effector (or equivalently, the force which the end-effector applies to the environment) can be computed directly from measurements of the motor torque after factoring in the inertial, Coriolis & centrifugal, and gravitational contributions stemming from the dynamic equations of motion. The motors only provide measured current, thus the torque at the actuator is:

$$\tau_m = K_\tau(i - i_0) \quad (37)$$

where K_τ is the torque constant from the manufacturer, while i and i_0 represent the measured and idle motor currents respectively. Unfortunately, the measured motor current can be quite noisy, thus directly resulting in noisy torque values. Inaccuracies in the torque constant would also lead to erroneous torque values, for which a Kalman filter is implemented. The methodology incorporated here follows that of Wahrburg et al. [28], in which the concept of generalized momentum is used:

$$\mathbf{p} = \mathbf{M}\dot{\mathbf{q}} \quad (38)$$

where \mathbf{M} is the inertia matrix computed in Section IV-E. By using this formulation, it can easily be seen that the derivative of the generalized momentum, $\dot{\mathbf{p}}$, simply equates to the equations of motion of the system:

$$\dot{\mathbf{p}} = \mathbf{M}\ddot{\mathbf{q}} = \boldsymbol{\tau}_m - \boldsymbol{\tau}_{ext} - \mathbf{C}(\mathbf{q}, \dot{\mathbf{q}})\dot{\mathbf{q}} - \mathbf{G}(\mathbf{q}) \quad (39)$$

For the state estimation task, we define a state vector consisting of the generalized momenta and the force vector at the end-effector, i.e. $\mathbf{x} = [\mathbf{p} \ \mathbf{F}]^T$. We can also define the input vector to the system as the compound torque consisting of the measured motor torque and contributions due to the gravity vector and Coriolis & Centrifugal term. For brevity, we will denote this term as $\bar{\boldsymbol{\tau}}$ such that:

$$\mathbf{u} = \bar{\boldsymbol{\tau}} = \boldsymbol{\tau}_m - \mathbf{C}(\mathbf{q}, \dot{\mathbf{q}})\dot{\mathbf{q}} - \mathbf{G}(\mathbf{q}) \quad (40)$$

Using the system's Jacobian which we defined earlier, this gives us the following equation for the generalized momentum's time derivative:

$$\dot{\mathbf{p}} = -\mathbf{J}^T \mathbf{F} + \bar{\boldsymbol{\tau}} \quad (41)$$

Looking at the other component of the state vector, namely the applied force, we can simply equate its time derivative to zero ($\dot{\mathbf{f}} = \mathbf{0}$) as the force will remain unaffected by the states.

Using the full state vector, this can easily be written in the form of a linear state equation:

$$\dot{\mathbf{x}} = \boldsymbol{\Phi}\mathbf{x} + \boldsymbol{\Gamma}\mathbf{u} \quad (42)$$

where:

$$\boldsymbol{\Phi} = \begin{bmatrix} \mathbf{0} & -\mathbf{J}^T \\ \mathbf{0} & \mathbf{0} \end{bmatrix} \quad (43)$$

$$\boldsymbol{\Gamma} = \begin{bmatrix} \mathbf{I} \\ \mathbf{0} \end{bmatrix}$$

Using the computed inertia matrix, we can directly measure the generalized momentum, yielding the following measurement equation:

$$\mathbf{z} = \mathbf{p} = \mathbf{H}\mathbf{x} \quad (44)$$

where

$$\mathbf{H} = [\mathbf{I} \ \mathbf{0}] \quad (45)$$

With this formulation, it is clear that the system can be expressed as a linear system of equations, enabling the use of a linear Kalman filter to estimate the applied force at the end-effector.

D. Position-Based Impedance Controller

A position-based impedance controller aims to indirectly control the force applied by a manipulator on its environment by adjusting the commanded position. This is done by virtually modelling the system as a mass-spring-damper such that we can control the mechanical impedance of the system.

In the *task space* formulation of the dynamics, we can express the mechanical impedance relationship as:

$$\mathbf{M}(\ddot{\mathbf{x}} - \ddot{\mathbf{x}}_0) + \mathbf{D}(\dot{\mathbf{x}} - \dot{\mathbf{x}}_0) + \mathbf{K}(\mathbf{x} - \mathbf{x}_0) = \mathbf{h} \quad (46)$$

where \mathbf{M} , \mathbf{B} , and \mathbf{K} denote the system's inertia, damping, and stiffness matrices respectively. Here in the general case, \mathbf{h} denotes the external wrench acting at the end-effector which comprises of the three force elements and the three torque elements (i.e. $\mathbf{h} = [\mathbf{F} \ \boldsymbol{\tau}]^T$). In the case of the Omni-Drone aerial manipulator, we have a single point of contact, thus there are no torques acting through the end-effector. Further, due to the planar design of the manipulator, we do not have control of the manipulator in the out-of-plane direction. Thus, we can simplify the wrench to a 2D force vector consisting of the radial (pointing outward from the point of contact) and tangential (pointing orthogonally to the right) force components at the end-effector. In equation (46) above, we note the inclusion of \mathbf{x}_0 and its time derivatives. These variables denote the desired reference values of the end-effector's position which would be tracked in the case of no interaction force. For the case of a static interaction, we can set the desired accelerations and velocities to zero and set the reference position to the desired position in the case of no interaction. Lets call this \mathbf{x}_d such that $\mathbf{x}_0 = \mathbf{x}_d$. Using position feedback, we can then compute the position error as $\mathbf{x}_e = \mathbf{x} - \mathbf{x}_d$. After some rearranging, we can then get the following control law:

$$\ddot{\mathbf{x}}_c = \mathbf{M}^{-1}(\mathbf{F} + \mathbf{K}\mathbf{x}_e - \mathbf{D}\dot{\mathbf{x}}_e) \quad (47)$$

Finally, equation (47) can be twice integrated to obtain the commanded position \mathbf{x}_c . Note that \mathbf{x}_c is a deviated position from the desired position \mathbf{x}_d . We can then apply inverse kinematics on this commanded position to obtain the motor position commands.

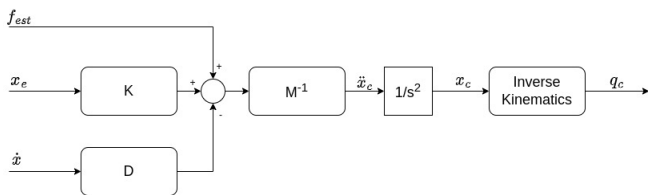


Fig. 7: Impedance Control Block



Fig. 8: Bench test setup

VII. STATIONARY EXPERIMENTS

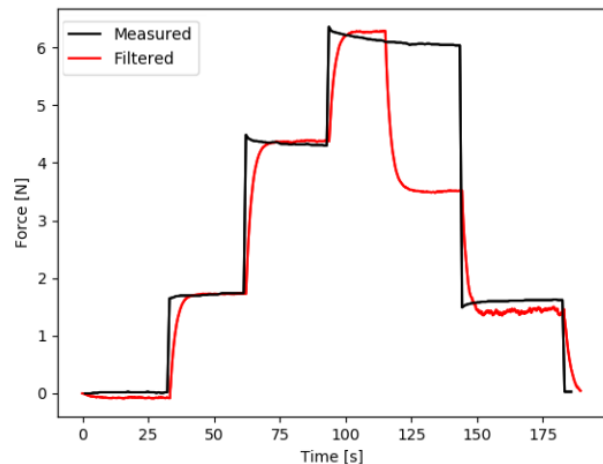
A. Setup

Prior to implementing the impedance controller, the force estimator is validated without the need for the drone platform. The manipulator is set up for stationary experiments by mounting it between two surfaces with sufficient space for it to rotate. The motors are connected in series to a 12V power supply from one end. The other end connects to a PC through the Dynamixel U2D2 converter. Also mounted between the two surfaces is a load cell that is to be used to measure the true force being applied through the manipulator's end-effector. The load cell is wired to an HX711 load cell amplifier, which is in turn wired to a RaspberryPi 3b to record the data. Figure 8 shows the setup of the bench test with the manipulator extended out laterally, making contact with the load cell.

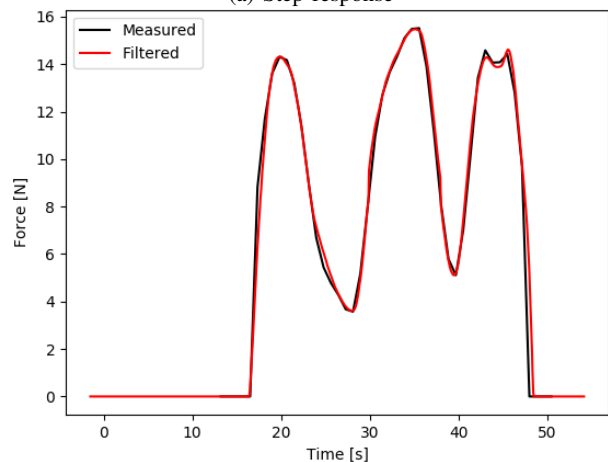
The manipulator is first commanded to incremental positions beyond the surface of the sensor. The sensor plate acts as the environment surface and restricts the manipulator from truly reaching its desired position. Because of this, as the manipulator attempts to reach further beyond the surface of the sensor plate, it will apply higher loads. A second experiment is then conducted where the manipulator is commanded to a constant reference position, similar to how it would be kept in flight. The sensor plate is then dynamically loaded by manually pushed against the end-effector such that it is loaded and unloaded periodically.

B. Results

Here we present the results of the two stationary experiments. Figure 9(a) shows both the measured ground truth (in black) and estimated force (in red) values. As can be seen



(a) Step response



(b) Dynamic loading

Fig. 9: Stationary experiment validation of the onboard force state estimator capabilities through step response (a) and dynamic loading (b).

from the force measurement, the force experienced at the end-effector incrementally grows with each step command as the manipulator attempts to reach further into the plate. From a preliminary glance, it can be seen that the force estimate is capable of tracking various values of applied force during the first half of the experiment.

The manipulator was then commanded to incrementally retract, back from the sensor plate, thus alleviating the applied force. Interestingly, as can be seen in the data plot, the applied force as measured by the load cell does not seem to decrease during the first retraction step. The torque in the motors decreases, thus the estimate decreases accordingly, however the actual applied force stays relatively the same. This behaviour was experienced repetitively. It is hypothesized that this behaviour could be due to friction in the Dynamixel motors, where the current is decreased correctly to account for the reduced position error, however the reduction in motor torque is compensated by a frictional torque.

This inaccuracy is alleviated in the dynamic loading experiment. Figure 9(b) presents the results of this validation

test with the measured force in black and the estimated force in red. We see that the performance of the estimator here is greatly ameliorated as it is able to closely track the dynamically changing load. This scenario is more closely related to what would be experienced in flight as change in the applied load is typically expected to be due to the change in the environment surface relative to the end-effector.

VIII. FLIGHT EXPERIMENTS

A. Setup & Outline

For performing the aerial interaction task, a concave surface, similar to a quarter-pipe, was constructed using Plexiglas mounted to a wooden frame and given an arbitrary, unknown curvature. Knowledge of the curvature is unnecessary as the manipulator's impedance controller is intended to maintain the contact force regardless of the surface geometry.

The UAV is equipped with a Pixhawk PX4 autopilot which communicates with an onboard RaspberryPi 4. The RaspberryPi in turn communicates with a Vicon motion capture system via MAVROS to provide feedback of the drone states. Control of the UAV's flight is performed manually through a remote controller in position-hold mode.

The vehicle is commanded to a given position by the operator. After contact is established with the contoured surface, the end-effector's motion is commanded such that the manipulator rotates in the direction of the curved surface, while maintaining the contact force through extension/retraction.

B. Results

We now present the results obtained from the aerial interaction task. Our interest lies in how well the controller is capable of tracking a constant applied force, and thus maintaining contact on the surface, as the manipulator is commanded to rotate along the surface of the contour. Figure 11 presents the aerial interaction data measured in the flight experiments. The figure shows the estimated force, obtained from the generalized momentum Kalman filter and the angular position profile of the pivot joint over time. Here, we can see that the manipulator was initially commanded to -90° to begin the interaction. It is then rotated down to roughly -150° before being commanded back to its initial position at -90° .

Observing the results of the force tracking, we see that the system is initially able to maintain a roughly steady force tracking, around $5N$. During this time, the attitude of the drone is relatively stable, with some oscillation in the yaw angle as can be seen in Figure 12. It is important to note that the roll angle ϕ is non-zero, holding steady around 2° . The reason for this is due to the fact that the UAV must counteract the force being applied through the manipulator and therefore must tilt toward to the surface to provide an equal reaction force. This is maintained as the manipulator rotates downward, following the contour, until q_5 is about 125° . At this point, we see the force decrease rapidly before increasing again and overshooting. We can get a hint of what may be going on by looking at the flight data of the drone platform.

Looking at the roll angle, we see that it quickly drops to zero at this stage. The reason for this is likely due to the

fact that as the manipulator rotates below the UAV, the lateral force which it had previously imposed quickly diminishes. As such, the UAV suddenly corrects for this absence of force, but in this process, pulls the manipulator away from the surface. The manipulator impedance controller attempts to correct for this loss, but overshoots in doing so until it finally corrects itself. At this stage, we also note an increase in the yaw angle oscillation as the UAV struggles to cope with the varying applied force through this pivot point.

IX. FUTURE WORK

The work of this paper aimed at developing a sensorless force estimator for a drone-mounted five-bar parallel manipulator. As shown, this force estimator could then be integrated with an impedance controller to perform aerial interaction tasks on unknown curved surfaces. The controller was used to autonomously contour follow in one direction so as to maintain contact with an unknown surface and track a constant force. To further develop the Omni-Drone platform to conduct contact-based inspection tasks, various stages of the operation can be automated. The force estimator can itself be used as a trigger to detect contact by setting a minimum force threshold. With this in place, it would be possible to automate the sweeping motion of the manipulator such that it traverses along the surface automatically, then have the drone subsequently move laterally along the surface along a path trajectory to explore larger regions.

From a controller perspective, it would be possible to augment the impedance controller to include adaptability so as to optimize the manipulator's behaviour in various environments. Various works have developed different adaptation strategies for the impedance parameters, effectively changing the dynamics of the system to behave either more stiffly or compliantly depending on the force being applied on the manipulator. An interesting implementation of this is presented by Roveda and Piga [29] on an industrial manipulator where the stiffness and damping parameters of the control system are increasingly adapted as the force error tends to zero. This allows the manipulator to act rather compliantly prior to contact and progressively become stiffer as the applied force approaches its desired magnitude. This same methodology could potentially be applied to the Omni-Drone aerial manipulator, using the force estimate, rather than a direct force measurement, for the adaptation laws.

X. CONCLUSION

In this thesis, we developed an omni-directional aerial manipulator based on the concept design by Hamaza & Kovac [11]. The system equipped a quadrotor with a rotating five-bar parallel manipulator to perform contact-based inspection tasks. To avoid the need for additional force sensors at the end-effector, we have employed a force estimation scheme based on the generalized momentum of the system and the torque feedback of the actuating motors. This force estimation scheme was validated by means of stationary test and has been shown to reliably track the true force applied at the end-effector.

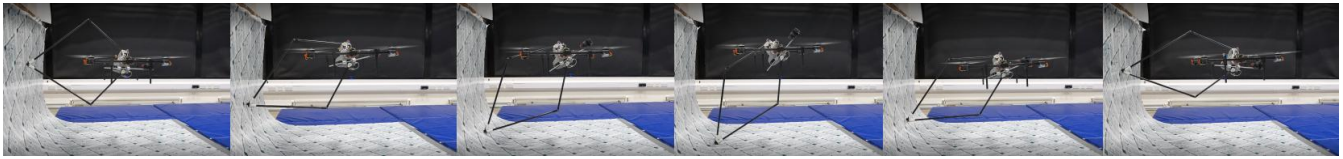


Fig. 10: Aerial interaction over time

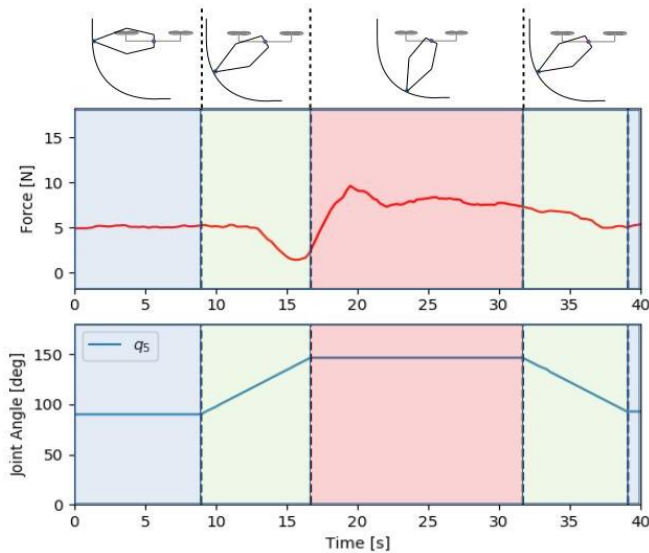


Fig. 11: Results of aerial interaction. Plot 1 presents the estimated normal force. Plot 2 presents the joint angle q_5 as the manipulator rotates down along the surface and back up.

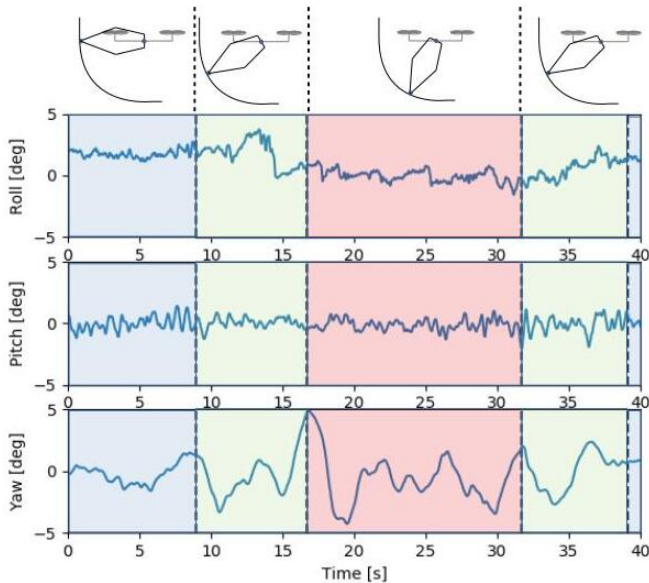


Fig. 12: Drone attitude data during the interaction task.

Using this force estimation in place of force feedback, we have implemented a position-based impedance controller to command the position of the manipulator's end-effector. The purpose of this controller was to maintain contact of the end-effector with unknown contoured surfaces while ensuring that

a constant force is applied. It was shown that in flight, the system was able to hold a relatively stable contact with the surface, however the vehicle platform would become unstable especially when the end-effector is located below the UAV due to the sudden change in direction of the resulting force being applied to the vehicle's body.

Further development into this system can potentially lead to its implementation for surface inspection tasks of complex surfaces. Its mechanical design affords it the ability to work within various task spaces and the controller implementation, with further work, could be used to maintain sensor contact without a-priori knowledge of the environment.

REFERENCES

- [1] F. Ruggiero, V. Lippiello, and A. Ollero, "Aerial manipulation: A literature review," vol. 3, no. 3, pp. 1957–1964, conference Name: IEEE Robotics and Automation Letters.
- [2] S. Gholizadeh, "A review of non-destructive testing methods of composite materials," vol. 1, pp. 50–57. [Online]. Available: <https://linkinghub.elsevier.com/retrieve/pii/S2452321616000093>
- [3] S. Hamaza, I. Georgilas, and T. Richardson, "2d contour following with an unmanned aerial manipulator: Towards tactile-based aerial navigation," in *2019 IEEE/RSJ International Conference on Intelligent Robots and Systems (IROS)*, pp. 3664–3669, ISSN: 2153-0866.
- [4] X. Meng, Y. He, and J. Han, "Design and implementation of a contact aerial manipulator system for glass-wall inspection tasks," in *2019 IEEE/RSJ International Conference on Intelligent Robots and Systems (IROS)*, pp. 215–220, ISSN: 2153-0866.
- [5] D. Zhang, R. Watson, G. Dobie, C. MacLeod, and G. Pierce, "Autonomous ultrasonic inspection using unmanned aerial vehicle," in *2018 IEEE International Ultrasonics Symposium (IUS)*, pp. 1–4, ISSN: 1948-5727.
- [6] H.-N. Nguyen and D. Lee, "Hybrid force/motion control and internal dynamics of quadrotors for tool operation," in *2013 IEEE/RSJ International Conference on Intelligent Robots and Systems*, pp. 3458–3464, ISSN: 2153-0866.
- [7] K. Bodie, M. Brunner, M. Pantic, S. Walser, P. Pfändler, U. Angst, R. Siegwart, and J. Nieto, "An omnidirectional aerial manipulation platform for contact-based inspection." [Online]. Available: <http://arxiv.org/abs/1905.03502>
- [8] —, "Active interaction force control for contact-based inspection with a fully actuated aerial vehicle," vol. 37, no. 3, pp. 709–722, conference Name: IEEE Transactions on Robotics.
- [9] M. Trujillo, J. R. Martínez-de Dios, C. Martín, A. Viguria, and A. Ollero, "Novel aerial manipulator for accurate and robust industrial NDT contact inspection: A new tool for the oil and gas inspection industry," vol. 19, no. 6, p. 1305, number: 6 Publisher: Multidisciplinary Digital Publishing Institute. [Online]. Available: <https://www.mdpi.com/1424-8220/19/6/1305>
- [10] F. Huber, K. Kondak, K. Krieger, D. Sommer, M. Schwarzbach, M. Laiacker, I. Kossyk, S. Parusel, S. Haddadin, and A. Albu-Schäffer, "First analysis and experiments in aerial manipulation using fully actuated redundant robot arm," in *2013 IEEE/RSJ International Conference on Intelligent Robots and Systems*, pp. 3452–3457, ISSN: 2153-0866.
- [11] S. Hamaza and M. Kovac, "Omni-drone: on the design of a novel aerial manipulator with omni-directional workspace," in *2020 17th International Conference on Ubiquitous Robots (UR)*, pp. 153–158, ISSN: 2325-033X.

- [12] S. Kim, S. Choi, and H. J. Kim, "Aerial manipulation using a quadrotor with a two DOF robotic arm," in *2013 IEEE/RSJ International Conference on Intelligent Robots and Systems*, pp. 4990–4995, ISSN: 2153-0866.
- [13] G. Heredia, A. Jimenez-Cano, I. Sanchez, D. Llorente, V. Vega, J. Braga, J. Acosta, and A. Ollero, "Control of a multirotor outdoor aerial manipulator," in *2014 IEEE/RSJ International Conference on Intelligent Robots and Systems*, pp. 3417–3422, ISSN: 2153-0866.
- [14] M. Tognon, B. Yüksel, G. Buondonno, and A. Franchi, "Dynamic decentralized control for protocentric aerial manipulators," in *2017 IEEE International Conference on Robotics and Automation (ICRA)*, pp. 6375–6380.
- [15] J. Thomas, J. Polin, K. Sreenath, and V. Kumar, "Avian-inspired grasping for quadrotor micro UAVs," in *Volume 6A: 37th Mechanisms and Robotics Conference*. American Society of Mechanical Engineers, p. V06AT07A014. [Online]. Available: <https://asmedigitalcollection.asme.org/IDETC-CIE/proceedings/IDETC-CIE2013/55935/Portland,%20Oregon,%20USA/252975>
- [16] L. Villani and J. De Schutter, "Force control," in *Springer Handbook for Robotics*, 2nd ed. Springer, pp. 195–220.
- [17] T. Bartelds, A. Capra, S. Hamaza, S. Stramigioli, and M. Fumagalli, "Compliant aerial manipulators: Toward a new generation of aerial robotic workers," vol. 1, no. 1, pp. 477–483, conference Name: IEEE Robotics and Automation Letters.
- [18] A. Suarez, G. Heredia, and A. Ollero, "Physical-virtual impedance control in ultralightweight and compliant dual-arm aerial manipulators," vol. 3, no. 3, pp. 2553–2560, conference Name: IEEE Robotics and Automation Letters.
- [19] M. Car, A. Ivanovic, M. Orsag, and S. Bogdan, "Position-based adaptive impedance control for a UAV," in *2018 International Conference on Unmanned Aircraft Systems (ICUAS)*, pp. 957–963, ISSN: 2575-7296.
- [20] L. Marković, M. Car, M. Orsag, and S. Bogdan, "Adaptive stiffness estimation impedance control for achieving sustained contact in aerial manipulation," in *2021 IEEE International Conference on Robotics and Automation (ICRA)*, pp. 117–123, ISSN: 2577-087X.
- [21] K. Lee and M. Buss, "Force tracking impedance control with variable target stiffness," vol. 41, no. 2, pp. 6751–6756. [Online]. Available: <https://www.sciencedirect.com/science/article/pii/S1474667016400285>
- [22] W. Lu, H. Liu, X. Zhu, X. Wang, and B. Liang, "Variable stiffness force tracking impedance control using differential-less method," in *2017 29th Chinese Control And Decision Conference (CCDC)*, pp. 4906–4911, ISSN: 1948-9447.
- [23] L. Roveda and D. Piga, "Sensorless environment stiffness and interaction force estimation for impedance control tuning in robotized interaction tasks," vol. 45, no. 3, pp. 371–388. [Online]. Available: <http://link.springer.com/10.1007/s10514-021-09970-z>
- [24] P. Cieślak and P. Rıdao, "Adaptive admittance control in task-priority framework for contact force control in autonomous underwater floating manipulation* this work is part of a project titled "force/position control system to enable compliant manipulation from a floating i-AUV", which received funding from the european union's horizon 2020 research and innovation programme, under the marie skłodowska-curie grant agreement no. 750063." in *2018 IEEE/RSJ International Conference on Intelligent Robots and Systems (IROS)*, pp. 6646–6651, ISSN: 2153-0866.
- [25] J. Buzzato, A. Hernandez, M. Becker, and G. d. P. Caurin, "Aerial manipulation with six-axis force and torque sensor feedback compensation," in *2018 Latin American Robotic Symposium, 2018 Brazilian Symposium on Robotics (SBR) and 2018 Workshop on Robotics in Education (WRE)*, pp. 158–163.
- [26] R. E. Kalman, "A new approach to linear filtering and prediction problems," vol. 82, no. 1, pp. 35–45. [Online]. Available: <https://doi.org/10.1115/1.3662552>
- [27] S. Fakoorian, V. Azimi, M. Moosavi, H. Richter, and D. Simon, "Ground reaction force estimation in prosthetic legs with nonlinear kalman filtering methods," vol. 139, no. 11. [Online]. Available: <https://doi.org/10.1115/1.4036546>
- [28] A. Wahrburg, J. Bös, K. D. Listmann, F. Dai, B. Matthias, and H. Ding, "Motor-current-based estimation of cartesian contact forces and torques for robotic manipulators and its application to force control," vol. 15, no. 2, pp. 879–886, conference Name: IEEE Transactions on Automation Science and Engineering.
- [29] L. Roveda, "Adaptive interaction controller for compliant robot base applications," vol. 7, pp. 6553–6561, conference Name: IEEE Access.

3

Literature Review

3.1. Introduction

The term aerial manipulator is given to an unmanned aerial vehicle (UAV) that is capable of physically interacting with its environment [4]. This is achieved through the integration of specific tools with a drone body that allow the vehicle to autonomously perform tasks such as scanning, grasping, and transportation of other objects. Though the field is premature, the ability to have these vehicles work autonomously around various structures paves the way to pursue implementations of drones for various tasks that would otherwise put humans in dangerous situations. Such tasks can include the inspections of industrial areas which could ideally be done in much safer and more efficient manners with aerial manipulators, especially when dealing with high-rise or difficult-to-reach structures. There is also the possibility to rely on these systems to perform tactile-based navigation to explore unknown regions in which visual cues may not be an option; for example if there is inadequate lighting.

3.1.1. Brief Overview of Non-Destructive Testing

As described by Gholizadeh, the field of non-destructive testing (NDT) involves the analysis of existing structures and components without causing damage or permanent change to the piece [5]. Many industrial lines of work, such as automotive, aerospace, and energy rely on NDT to inspect material properties and detect defects [6]. This field of NDT could see a significant contribution from the use of aerial manipulators. Since many of the scenarios regarding NDT are involved with large, complex structures, such as wind turbines, the risk to human operators could be greatly reduced by sending up an autonomous vehicle in their place.

The equipment needed to perform most NDT involves sensors that are capable of obtaining eddy current, magnetic, electromagnetic, and penetrant testing measurements [5]. For all of these listed methods, the corresponding sensor must be kept consistently in good contact with the inspected material surface in order to ensure that the obtained data is reliable. Though most NDT tasks are still being done by human operators, some advancements have been made to automate these tasks using systems such as wheeled robots, as described by Bogue [7]. The article goes into an extensive review of various types of robotic NDT systems for different applications, including the testing of oil & gas equipment, power generation utilities, and aerospace/nautical equipment. Though these robotic systems are capable of detecting defects in the above-mentioned structures, each robot is specially designed for a particular task, making them quite expensive, and thus not typically abundant in most industries.

In order to perform these tasks using aerial vehicles, the systems would need to be able to maintain consistent contact with the environment without disrupting or destabilizing its own flight control. As will be discussed further on, there exists a limited number of works regarding the application of UAVs for NDT, such as by Car et al. [8], Zhang et al. [9], and Trujillo et al. [2], however they each possess limiting factors which could be greatly improved. By meeting the objectives set out in the following subsection, the proposed research will attempt to demonstrate the potential for future aerial NDT systems.

3.1.2. Recent Applications of Aerial Manipulators

Multiple implementations of aerial manipulators have been popping up in the research community as their potential becomes more apparent. Work by Hamaza et al. have proposed an aerial system that can perform surface interactions on a 2D environment [10]. The intention of the work is to demonstrate the potential to later perform NDT and/or tactile-based navigation. This is done by showcasing system's capability of maintaining contact with the environment surface while moving along tangentially. Similar work has also been accomplished by Meng et al. on an aerial vehicle fitted with a manipulator that is capable of performing both static and dynamic interaction with planar glass surfaces [11].

Expanding on this, NDT has been accomplished in a 2D setting, albeit to a limiting extent, using an aerial manipulator in the work by Zhang et al. [9]. They present a UAV that is fitted with an ultrasonic sensor. The system is autonomously guided toward a 2D aluminum sample and takes measurements while maintaining contact. To do this however, the UAV follows a predefined trajectory based on accurate knowledge of the vehicle's and aluminum surface's respective positions. This would not be ideal in a true setting as it would require a full accurate model of every structure that is to be inspected by the system.

In progression from 2D, Bodie et al., have pursued research into three dimensional interactions in two complementing works [1], [12]. In the first, a fully-actuated drone is fitted with a manipulator

arm equipped with a wheel at its end-effector. The system is validated by tracing 3D contours of concrete surfaces, such as arch ways, while maintaining steady contact with tracking of a desired force. The second work performs similar tasks using a force-sensing rigid boom to better maintain the force tracking requirement. It is also integrated with an NDT sensor that measures electrical potential and electrical resistance. The authors present preliminary results of an inspection of a small concrete sample.

Continuing with fully-actuated aerial vehicles, Trujillo et al. developed an eight tilted-rotor drone with an active robotic manipulator for the specific purpose of performing NDT in the Oil & Gas industry [2]. The authors claim the system can operate with an omni-directional workspace thanks to its tilt-rotor design and was used to collect NDT measurements of industrial pipes. The system still requires a human operator to control its flight in free-space as well as during the inspection however; the on-board controller is only tasked with maintaining contact with the environment.

As will be later discussed in this report, aerial manipulation techniques have been tending toward systems with flight control systems with increasing complexity. Flight dynamics are generally non-intuitive and thus a desire exists to keep the control of the drone body as simple as possible.

In an effort to introduce an aerial manipulator with a general workspace, but with relatively simple flight control, Hamaza and Kovac have proposed a new system conceptual design [3]. This system, named Omni-Drone, consists of a conventional quad-rotor drone equipped with an active parallel five-bar manipulator attached to the vehicle's Centre of Mass (CoM). The paper claims that the system offers an omnidirectional workspace about the drone's body. To achieve this, radial extension and retraction is first attained through the actuation of the two base joints of the manipulator. Planar azimuthal motion is done by pivoting the entire manipulator linkage around the drone body. The final out-of-plane motion is then lastly achieved through the yaw-motion of the drone. Therefore, unlike the other works described above, this Omni-Drone is conceptually capable of performing aerial manipulation from any position relative to the environment, while depending on the vehicle motion for only a single Degrees of Freedom (DoF).

The research that is being proposed through this literature review will set out to implement the conceptual design proposed by Hamaza and Kovac. This intends to demonstrate the ability of applying desired forces while moving tangentially along general surfaces. Using the OmniDrone's pivoting manipulator, it is expected that it will be possible to perform these contact interaction tasks along surfaces of any orientation. As the following subsection will establish, the research intends to measure the the extent of the system's capabilities to perform these tasks.

3.1.3. Research Question

We wish to expand on the currently available research regarding aerial manipulation with the intention of consistently applying desired forces while traversing along arbitrary surfaces. To achieve this, we will attempt to answer the following question. **How accurately can a desired wrench be applied at the end-effector of an aerial manipulator without prior knowledge of the environment which it will be interacting with and without using a direct wrench sensor at the end-effector while traversing along the contour of the environment's surface?** To properly develop a system that answers this question, we must first look into how the aerial vehicle and the robotic manipulator can be integrated together and how smoothly the control allocation between the two can be transitioned. Further, before the force-tracking controller can be employed, validation of the system's force estimator will need to be conducted. To do so, it will be important to measure how closely the system can estimate the forces applied by the robotic manipulator and compare these estimates to true measured values. This will need to be validated against both smoothly changing inputs as well as step-inputs. This is because step-changes of the applied force will be experienced at the moments when contact is initiated and terminated. In parallel, it will be necessary to measure how well the flight controller will be able to maintain its desired trajectory amid the applied forces and torques due to the on-board manipulator's interaction with the environment. Answering each of these sub-questions will in conjunction formulate the necessary results to answer the primary research question stated above.

3.1.4. Literature Review Outline

The following will provide a review on the research regarding aerial manipulation within existing literature. It will be subdivided into four primary sections that each discuss an important aspect of designing an aerial manipulator for contact-based inspections. The first section provides an analysis of the sys-

tem architectures of existing aerial manipulators. Here, the various designs can fall under different classifications depending on the type of manipulator attached to the drone. This classification can then be further distinguished based on the setup of the system integration. This will lead into the second section where the differences between centralized and decentralized control architectures are discussed. Following this, the review examines the various control methodologies implemented for contact force-tracking tasks. In this section, not only will aerial manipulators be considered, but inspiration is also taken from other systems such as fixed-base manipulators. Here, focus will be put on the differences between direct and indirect force control strategies. This will then lead into deeper analyses of impedance control along with corresponding adaptation laws to account for unknown environment parameters. Finally, the report discusses the preference to avoid the use of external force/torque sensors at the end-effector of the manipulator. Because of this, force estimation techniques are then explored.

In concluding the review, the findings found in the various sections will be consolidated and a research gap is identified. The idea will be to draw methodologies from various sources, each contributing to a portion of the aerial manipulation design that will be pursued by the proposed research.

3.2. Aerial Manipulation

Research and development of UAVs has seen rapid growth in recent years as industries are beginning to realize the extent of their potential [13]. Up until recently, these UAVs were primarily used for passive tasks using visual systems (such as surveillance) and were incapable of performing environment interactions like their ground-constrained robotic counterparts. More recently however, the research community has begun to explore the idea of equipping these UAVs with tools to perform manipulation tasks while flying. As discussed by Ruggiero et al. [4], there are typically two contrasting approaches to accomplishing this: 1) attaching a rigid tool to the drone body; and 2) integrating an active robotic arm on the drone, which can have varying amounts of DoF.

3.2.1. Rigid Tools

In the case of rigid tools, a gripper or boom is attached to the UAV and the manipulation of objects is done solely through the flight control of the vehicle. An early example of this is presented by Mellinger et al. where the design of two types of grippers are proposed for the attachment to the bottom of a quadrotor drone [14]. The idea presented within the article is for the grippers to be used to either actively perch the drone for the benefit of endurance or to pick up and transport payloads through the air. The quad-rotor design is selected for its simplicity; however, it is noted in the paper that the inclusion of the gripper and additional payloads significantly changes critical flight parameters which then need to be estimated and compensated for. In order to account for this, the authors implemented a least squares parameter estimator to estimate the new mass and CoM of the drone (i.e. with added payload). These estimates were then fed to a flight controller which internally compensated for these changes. The drone was commanded to fly along a sine wave flight path and comparisons were made against a controller which did not include these compensating terms. Through this, significant improvements were achieved with the compensated controller, especially during instances where there are changing thrust commands.

In contrast to grippers, research has also gone into the interaction of aerial vehicles with environmental surfaces. The accomplishment of this kind of interaction paves the way for NDT using drones as autonomous tools capable of performing the inspections. Work by Smrcka et al. implemented an admittance controller based on the measured interaction force with a wall in order to stabilize their UAV on a lateral surface [15]. The purpose of this system is to perform visual documentation and inspection of poorly-lit historical buildings in cases where light sources need to be pressed up against the surface being inspected. The benefit afforded by this work is that they are capable of automatically approaching, contacting, and stabilizing with a surface in an environment which may not have access to Global Navigation Satellite System (GNSS) signals. The admittance controller allows the vehicle to safely make contact and maintain its position without tremendous impacts to the hardware or the environment.

A similar system structure has also been investigated for applications involving the dynamic interaction of an aerial vehicle with an environment structure. Nguyen and Lee present the design of a quadrotor drone with a static tool attached either to the top or the bottom of the vehicle [16]. By transforming the drone's dynamics to the tool's end-effector frame, the flight controller becomes capable of driving the tool's position to desired locations along the environment while maintaining desired forces. The issue that arises with this however is that quadrotors are inherently under-actuated and thus its operational space is drastically limited, especially in the pitch and roll directions. As will be discussed, this can be improved by either increasing the actuation capabilities of the vehicle or by introducing various levels of actuation on the manipulation tool itself.

This type of work has also been pursued using drones with greater manoeuvrability which has led to the potential of employing them in contact-based operations for NDT. As previously introduced, the work by Bodie et al. employs a fully actuated tilt-rotor system with a rigid boom mounted to the drone body [12]. The paper presents a control scheme for accurate interaction of the boom's end-effector over the surface of concrete infrastructure. Since the end-effector remains in a static position relative to the drone body, the kinematics become entirely coupled to the drone's flight control and thus could complicate the control system, hence the need for a fully actuated system. The control methodology used aboard this system will be later discussed in further detail in Section 4, however it is worth noting that the dexterity of the aerial manipulator can be improved by allowing the manipulator to move relative to the vehicle body and could potentially simplify the architecture of the entire system.

3.2.2. Active Robotic Manipulators

In contrast to the previously mentioned systems, the addition of active robotic arms could greatly increase the effectiveness of aerial manipulators. These robotic arms can have varying DoF. In these cases, the level of DoF can greatly influence the complexity of the flight control required to accomplish the manipulation task with adequate stability. By increasing the DoF, the manipulator's influence on the aerial vehicle can be reduced [17]. The downside to this however, as explained by Hamaza et al., is that this increase in the DoF introduces additional weight to the system, thus limiting the battery life and manoeuvrability [10]. For this reason, the system introduced in their work utilizes a single-DoF linear manipulator mounted to the top of their UAV. Through this, a desired interaction force can be applied onto a surface in front of the drone, without having to entirely rely on the drone's flight motion to make/remove contact nor adjust the normal force on the surface. Because of its limited DoF however, lateral and vertical motions relative to the surface must still be accomplished entirely by the flight controller.

The single-DoF linear manipulator approach can be augmented while still maintaining structural simplicity, by introducing an additional DoF. This can be seen through the work of Bartelds et al. where a similar structure incorporates a linear manipulator is mounted to the top of the drone, but now includes an active rotational joint near the attachment point [13]. This additional DoF allows the manipulator to compensate for the drone's pitch motion. The other DoF, in the linear direction, again allows the system to apply the desired normal forces on the surface while providing a certain level of compliance when in contact with the environment. Just like the previous work however, the system is still entirely reliant on the drone's flight control for motion of the end-effector in the lateral and vertical directions.

To achieve higher levels of dexterity, the DoF of the manipulator arm can be increased such as in the work of Kim et al. [18]. The paper introduces a quad-rotor drone equipped with a 2-DoF robotic arm, mounted to the belly of the vehicle, and with a mechanical gripper at the end-effector. The purpose of the system is to perform tasks involving the pick-up, delivery, and placing of small objects. Due to its design, the mechanical arm can be adjusted through the control of two active joints that allow the end-effector to be positioned through planar motion relative to the drone body. The design still has its limitations however, as lateral motions as well as roll and yaw of the end-effector still need to be entirely controlled by the drone's flight. Further, since the manipulator is mounted to the bottom of the vehicle, the drone is only able to interact with objects which it can approach from above.

A similar design methodology has been implemented by Huber et al. on-board an autonomous helicopter [17]. Like the work presented by Kim et al., the manipulator is again mounted to the bottom of the vehicle with a gripper at the end-effector. The intention of the system is for applications involving tasks such as aerial inspections, sampling, and delivery of supplies. Despite being attached from below, the manipulator consists of 7-DoF for the sake of achieving all 6-DoF of motion for the end-effector with redundancy. Though the manipulator is effectively unconstrained in terms of the motion directions afforded by the active joints, mechanical limitations are inherently imposed by the system's design. Once again, the fact that the manipulator is mounted from below means that the helicopter must approach the interaction environment from above. Further, the landing struts of the helicopter introduce physical boundaries which the robotic arm risks colliding with. Because of this, the implemented control system limits the motion of the manipulator within a virtual cage between these struts, and so the manipulator's true operation space is smaller than it would otherwise be.

Tognon et al. demonstrate the implementation of a light-weight manipulator arm mounted to the bottom of a quadrotor drone [19]. The manipulator has 2-DoF with a gripper mounted to its end-effector. The design is based on another work by Thomas et al. that develops an underside gripper for high-speed grasping tasks [20]. Both works are bio-inspired by the approach taken by birds-of-prey, such as eagles, and try to mimic their grasping motions during flight. The design of Tognon et al. is particularly interesting as the two motors that control the manipulator arm are directly mounted near the CoM of the drone. The first motor is directly attached to the joint regarding the first DoF, but the second motor is connected to the other joint via a metal-reinforced plastic belt. The reason for this is that the inertia of the manipulator arm is kept to be very low, meaning a relatively small quadrotor can be utilized for the application.

Peng et al. take this concept of a bottom-mounted manipulator even further and attempt to decouple the arm's motion from the drone's flight dynamics [21]. The system consists of a quad-rotor drone with a four-bar mechanical linkage attached to its underside. The main difference from the other works however is that this attachment is made via a gimbaled mechanism. As described by the paper, the

purpose of this arises from the fact that with most aerial manipulators, the motion of the UAV platform will often affect the positioning of the manipulator's end-effector, and vice-versa. The introduction of the gimbal is intended to allow the manipulator to stay still relative to inertial space even when the vehicle platform experiences disturbances to its intended position/motion.

These aerial vehicle designs with bottom-mounted robotic manipulators tend to be the most prominent in aerial manipulation as they provide the benefit of picking up and placing objects easily. An example of this includes the work of Heredia et al. where the robotic manipulator is equipped with a gripper and visual camera at the end-effector [22]. A similar design is presented by Cataldi et al. [23] with the intention of demonstrating its potential to be used for assembly and construction of structures. Thirdly, this concept of bottom-mounted manipulators is extended in the paper by Suarez et al. where a dual-arm system is integrated with an aerial vehicle to achieve more human-like control behaviour [24]. In all of these cases however, the task space of the system is limited to the region below the drone. This makes it difficult to perform interactions with structures like bridges, where it may be necessary to access them from below.

The physical limitations attributed to the previous works can be overcome through manipulator and/or vehicle design, depending on the intended application of the system. As touched upon in the introduction, this is observed through the development by Trujillo et al. [2] of an octo-rotor drone, named AeroX, for the sake of NDT inspections. The tool has been designed for specific inspections of structures in the oil and gas industry, using either eddy-current or ultrasonic sensors. The work claims that the system is capable of performing contact inspections in all directions and orientations. It does this by using a fully-actuated tilt-rotor drone equipped with an active parallel manipulator. The manipulator is capable of both extension/retraction motions as well as limited planar rotations about the drone body. This design means that general motion of the end-effector is controlled through the flight control of the drone, while precise fine-tuning of the end-effector's position for the sake of maintaining surface contact is done through the manipulator's motion. This introduces high-levels of complexity however, which may not be preferred in application settings. Furthermore, the use of AeroX requires remote-control of a fully-actuated tilt-rotor vehicle, introducing the need for a highly skilled operator. Here, the implemented control scheme simply maintains contact of the end-effector with the environment while the operator commands the drone to move along the surface. Thus, it is not an entirely automated system.

A similar inspection tool is also presented by Tognon et al. for NDT inspections of pipes [25]. The system consists of a hexarotor drone with tilted rotor arrangement that provides multidirectional thrust. Through its underside, the drone is equipped with a 2-DoF robotic manipulator. Together, the paper claims that the system achieves 8-DoF motion, thus yielding control of both the end-effector's position and orientation in all directions with some redundancy. The lengths of the manipulator's linkages are long enough to allow for upward interaction with the environment, despite its underside mounting. The work demonstrates the tool's ability to perform accurate eddy-current testing of metallic pipes. Despite its ability to perform interactions in upward directions, the system is still limited as the drone body must remain above the inspected object.

3.3. Centralized vs. Decentralized Control

When discussing aerial manipulators where the manipulator arm is actively controlled, the system can be characterized as either **centralized** or **decentralized control**. In the case of centralized methods, the UAV and the robotic arm are treated as a single coupled system. Due to this, the dynamics typically need to be computed specifically for the system in question, with dependencies on manipulator configurations, resulting in higher complexities from a control standpoint. In contrast, decentralized control schemes treat the robot manipulator independently from the UAV. Here, the resulting forces and moments due to the manipulator's motion and interaction with the environment are treated as external factors to the UAV's flight control; and vice versa. This allows the design of the aerial manipulator to be thought of in terms of two parts: 1) the flight control of the UAV; and 2) the control of a robotic manipulator.

3.3.1. Centralized Control

The previously introduced work by Kim et al. is a prime example of this centralized system [18]. The control system proposed for their design defines a state space of generalized coordinates including the position and attitude of the drone as well as the two joint angles attributed to the robotic manipulator. By doing so, the centralized dynamics are derived using the Lagrangian-D'Alembert equation.

Further, a more complex centralized control scheme is implemented on an aerial manipulator and is presented in the work of Heredia et al. [22]. The work focuses on the development of an octoquad UAV with a 7-DoF manipulator arm attached to the bottom of the vehicle frame. The dynamics of the system are formulated with a generalized state vector which includes the position and attitude of the UAV, along with the seven joint angles of the robotic arm. This leads to the forces and torques applied by the arm being directly included in the full system dynamics.

3.3.2. Decentralized Control

Referring back to the aerial manipulator of Tognon et al., a decentralized control scheme is defined between the quadrotor drone and its 2-DoF manipulator arm [25]. Here, given desired positions and attitudes for the drone and desired positions and torques for the manipulator's end-effector, the two systems are controlled completely independently. The attitude and position controllers work together to convert the desired attitudes and positions to thrust inputs to the drone. Simultaneously, the arm controller converts the end-effector's desired positions and torques to commanded joint positions and velocities. Their results demonstrate good tracking of the desired values, however the control of the aerial manipulator is done in free-space, without contact with the environment.

Though the transformations of desired reference signals to command signals are done independently, the system dynamics that compute these desired values are still coupled between the two systems. The authors employ a method called differential flatness to simultaneously compute both the reference signals for the drone as well as for the manipulator. This same strategy is pursued by Thomas et al. [20]. This method exhibits benefits when aerial manipulator must perform tasks where the drone body is undergoing high dynamic motion, however it introduces additional dependency on the flight controller. This is unnecessary especially in slow-moving tasks, such as inspections, where the drone's body is expected to traverse gradually if at all. In these cases, the drone body can be treated as a floating platform to which the manipulator is attached to.

The issue that arises with this decentralized school of thought is the introduction of the manipulator's singularities. A robotic manipulator will inherently have configurations which are either unreachable or inescapable due to its geometry. Compensations would need to be made to avoid these configurations. Looking at the system design of the aerial manipulator by Marković et al. one can see an interesting implementation of a decentralized system [26]. The authors acknowledge the physical limitations of the on-board manipulator attributed to its singularities at fully-extended and fully-retracted states. Due to this, the proposed system is capable of controlling the end-effector position either through the motion of the drone (i.e. moving the end-effector *along with* the drone body frame) or through the motion of the manipulator itself (i.e. moving the end-effector *relative* to the drone body frame). The choice methods is done through a binary selection parameter that is dependent on the Euclidian norm of the joint error from a predefined optimal joint position. When this norm exceeds a defined threshold, the control of the end-effector switches from being manipulator-controlled to being flight-controlled. There is room for improvement on this methodology however as it results in an on/off behaviour. One could possibly

employ a way to smoothly transition between the two states where control of the end-effector could be shared between the flight controller and manipulator controller during this transition period.

3.4. Control Methods

The following section outlines the various control methodologies that are presented in the literature for manipulation tasks. Assuming that preference is given to decentralized control architectures, the control of the vehicle itself (including the necessary disturbance rejection) will need to be considered in addition to control of the robotic manipulator. The following section will thus be broken into two parts. Firstly, direct and indirect force control methodologies will be explored, with further exploration into adaptive concepts for indirect force control. Secondly, a brief overview of control strategies of floating platforms will be presented. This section primarily explores how other similar design structures handle the influences of external manipulation on their vehicle control.

3.4.1. Manipulator Control

Manipulator Compliance

As previously mentioned, the proposed research will need to apply maintained contact through the aerial manipulator's end-effector on the environment surface. Further, it may be required that a specified reference force vector is tracked. As described by Villani and De Schutter, this kind of interaction introduces kinematic constraints to the workspace and because of this, pure motion control (i.e. position, velocity, and/or acceleration control) will be insufficient [27]. In fact, the implementation of motion control in these situations may lead to potential damage of the manipulator and/or the environment. The authors continue to explain that control of a manipulator in these constrained environments must be accomplished with some sort of compliance. This compliance effectively allows the manipulator to conform to the imposing constraints to a certain extent and can be achieved through either passive or active interaction control methodologies.

When discussing passive interaction control, the compliance of the system is attained directly through the flexibility/admittance of the structure [27]. An example of this mechanical compliance is given in the work by Bartelds et al. [13]. As already previously introduced, the system consists of a single-DoF manipulator which allows the system to apply interaction forces laterally. Mechanical compliance is achieved by means of an elastic band that acts as a spring and stores kinetic energy induced by impacts with the environment into potential energy. A mechanical locking mechanism restricts this compliant motion in a single direction so that the energy is stored permanently in the band until a release lever is triggered manually. The authors perform experimental compensation between this compliant manipulator and an entirely rigid manipulator to demonstrate the effects of the impact with a planar surface in both cases. As expected, the compliant behaviour afforded by the elastic band allows the drone to make steady, consistent contact with the wall, with negligible bounce and pitch error. Though this design successfully demonstrates its intended use, it would be insufficient for general interactions. The use of the elastic band on the linear manipulator only provides compliance along the normal force direction. It would not yield to forces along the tangential directions of the interaction nor to torques applied at the end-effector. Therefore, the proposed design would not be able to properly deal with push-and-slide tasks where the end-effector would need to trace the contour of a surface while maintaining contact.

In contrast to passive interaction control, active control methodologies can also be implemented where the compliance of the system is achieved through a programmed control system. As explained by Villani and De Schutter, this often requires measurement of the contact wrench which is then fed back to the controller [27]. This can be done through either direct or indirect force control. The differences between these two methods will subsequently be explained along with examples of their application throughout the literature. For this, not only applications in aerial manipulation will be explored, but also works done in the fields of industrial robotics and underwater autonomous vehicles.

Direct Force Control / Hybrid Position-Force Control

Direct force control methods, as the name implies, attempt to apply a desired wrench by adjusting the forces and torques at the end-effector through the relationship between the end-effector and the joint torques. When this force needs to be applied along a surface while moving through space, the task must be explicitly and accurately defined. This is because both the force and the motion reference signals are independently fed to the control algorithm. The most prominent method for these kinds of applications was developed by Raibert and Craig and is named *Hybrid Position/Force Control* [28]. The method effectively divides the task space into the constrained (force control) directions and the

unconstrained (motion control) directions. Doing so allows for the simultaneous control of both force application and motion.

The work by Nguyen and Lee demonstrates the implementation of a hybrid position/force controller on a quadrotor aerial manipulator equipped with a rigid tool [16]. The intent of their research is to have the aerial manipulator trace a path along a given surface while maintaining 1N of contact force. The authors identify one limiting constraint of the hybrid position/force control method which stems from the requirement that the end-effector must always be in contact with the surface. This is clearly an undesirable constraint since the drone must be able to take off and approach the wall before contact can be established. To work around this issue, the work utilizes a technique called *passive decomposition* which effectively decomposes the dynamics into tangential and normal components relative to the surface. Accurate force and position tracking is demonstrated through simulation, however it is shown that stability of the system is only guaranteed when the tool is mounted to the top of the drone; thus limiting its reachable space.

An example of a hybrid position/force controller is presented in the work by Dong et al. where the controller is implemented on an industrial robotic polishing tool [29]. In the motioncontrolled subspace, the controller attempts to track desired position, velocity, and acceleration using a proportional-derivative (PD) control law. Conversely, the force-control subspace tracks a defined normal force reference signal using a proportional-integral (PI) controller. The authors explain their choice of PD and PI control due to the need for a fast dynamic response in motion, but a smooth and accurate tracking of force respectively. The resulting commanded acceleration and force signals are then converted to desired joint torques and passed to the motor controllers for execution.

The control method has also been implemented on a continuum robot by Xu et al. [30]. Like with other hybrid position/force control methods, the interaction space is divided into the constrained force space and the unconstrained motion space. The authors present a new modification to the control scheme where the commanded position signal is adjusted based on the deformations of both the environment and the robot itself due to their own respective compliance. This is done by treating both the environment and the robot as ideal elastic bodies with their own spring constants. The force error signal is then split and multiplied by the environment stiffness and the robot stiffness to obtain the resulting deformations. The environment deformation is then added to the desired position signal while the robot deformation is subtracted. Though their results show accurate tracking of the desired force, the position error tends to diverge, especially with higher applied forces. Further, the way the control scheme is set up would require accurate knowledge of both the environment's and robot's stiffness. Though this may be feasible for the robot, the environment stiffness would be case-specific and may not always be accurately known.

As previously mentioned, the use of hybrid position/force control requires accurate knowledge of the task space since the end-effector's motion through space must be explicitly commanded. Jatta et al. propose a modification that allows the method to better be used for tracing unknown contours [31]. Rather than commanding the end-effector's position in Cartesian space, a desired tangential velocity is given directly as reference to the controller. The controller is implemented on an industrial robotic manipulator with 2-DoF. The proposed scheme on the motion-control side takes a desired tangential velocity and implements a proportional-integral-derivative (PID) controller on the error signal. The desired tangential velocity is also provided as a feed-forward signal (with proportional gain) that is then summed with the PID output. On the force-control side, the normal force error is supplied to a PI controller and the reference signal is again feedforward (with proportional gain) to be summed with the PI controller's output. The resulting control signals are then fed through inverse kinematics to yield the commanded joint torques. The results showed high oscillations in the resulting applied force. In an effort to attenuate this, a modification to the controller was made which introduced a feedback loop on the normal velocity with the intention to drive it to zero. Though it successfully attenuates the oscillations to an extent, it does not completely eliminate them.

Indirect Force Control / Impedance (Admittance) Control

Contrary to the hybrid position/force control method discussed above, indirect force control does not contain an explicit feedback loop for the contact force. The most popular method of achieving this is through impedance control (or equivalently, admittance control). As explained by Villani and De Schutter, the end-effector's deviation from the defined desired motion is directly related to the experienced contact wrench with the environment [27]. This relationship is defined by the mechanical impedance

of the system and is obtained by modelling the system as a mass-spring-damper. Like in the previous section, impedance control has been widely implemented throughout multiple fields of robotics, including aerial manipulation. The following will outline several of these implementations, highlighting their similarities and differences, leading to the gaps left by the existing literature.

As mentioned earlier, one of the critical aspects of aerial manipulation is the compliance of the end-effector. Recall that without compliance, the manipulator would be too rigid and could possibly cause damage to the hardware and/or the environment upon contact. Suarez et al. have developed a dual-arm aerial manipulator for pipe inspections that includes both passive and active compliance methods [24]. The passive compliance is simply achieved through a pair of standard springs at each of the manipulator joints. More interestingly however is the active compliance induced by the variable impedance controller applied to the system. To do this, the controller defines the joint torque signals as a function of the end-effector position and velocity errors with respect to stiffness, damping, and inertia matrices that make up the mechanical impedance model. Several validation experiments are performed using the manipulator with this control scheme including contact force control and grasping tasks. In all cases, the stiffness and damping matrices had to be experimentally tuned for the application. Though the force tracking is done relatively well, this standard impedance controller would be insufficient in unknown environments where the controller parameters cannot be experimentally tuned beforehand. For this, self-tuning control methods will be required.

Adaptive Impedance Control

In these cases where the interacting environment is unknown, the parameters of an impedance controller need to be adjusted according to measurements that are fed back to the controller. This draws the requirement for so-called adaptive impedance controllers. The work by Car et al. demonstrates the improvements afforded by adaptive impedance control over its non-adaptive counterpart in the case of aerial manipulation [32]. The control method is established in the one-dimensional case where the aerial manipulator's end-effector is commanded to push down on a planar surface below the drone with a contact force of 2N. By first implementing a classical impedance controller, the authors numerically show that the steady-state force error can only be driven to zero with perfect knowledge of the environment stiffness and position; and that even small errors in either of these values can lead to large steady-state errors. To fix this, the work introduces an adaptation law that uses the measured force error to compute the reference position which is then fed to the impedance controller. This is done using time-varying proportional and derivative gains on force error along with an additional auxiliary signal that compensates for the steady-state error. These gains are then computed by relating the reference position signal to the actuator dynamics and deriving the necessary gain values to achieve a desired performance. This is based on a second-order dynamic model with user-defined damping and natural frequency. Simulations are conducted for both the non-adaptive and adaptive impedance controllers for the application of both constant reference forces as well as reference forces with step-changes over time. As expected, the adaptive impedance controller outperforms the classical controller, especially when the required force is changing. Two major concerns do arrive with this methodology, however. Firstly, since the adaptive laws are modelled about a second-order dynamic model, it will inherently yield oscillatory behaviour around the desired applied force value. Secondly, the derivation of the proportional and derivative gains presented by the authors yield parameterized equations, for which these parameters must still be experimentally tuned.

The impedance controller employed by Marković et al. introduces an adaptive parameter which regulates the reference position signal with the intention of driving the resulting steady-state force error to zero [26]. The function definition of this adaptive parameter is based on the force error, its derivative, and an additional auxiliary term which compensates for the impedance behaviour of the interaction. This definition is set up in such a way that when the adaptive parameter converges, it is inversely equal to the environment stiffness value; thus numerically validating the ideal force-tracking behaviour at steady state. Though the adaptation law presented in the paper yields an ideal-case adaptation law, it requires the solution of a third-order differential equation. These high derivatives are numerically expensive and can easily lead to large errors in the presence of noise.

Cieslak and Ridaou pursue a similar train of thought with the adaptive admittance controller employed on their autonomous underwater vehicle equipped with a 4-DoF manipulator arm [33]. The system takes a desired end-effector position and contact wrench as input to the admittance controller and outputs a modified end-effector position signal based on a virtual mass-spring-damper model. As

discussed before, this mass-spring-damper model consists of mass, damping, and stiffness matrices that define the dynamic behaviour of the system. Since this method on its own does not provide direct control over the contact wrench which could suffer from significant errors due to unknown environment characteristics. To account for this, the work proposes to adapt the virtual stiffness matrix over time as an integral term of the wrench error with an appropriate gain applied. Through experiment on an underwater pipe, this simplified adaptation model demonstrated rapid response to a step change in the desired force signal, however the resulting applied force through the end-effector exhibited extremely high oscillatory behaviour.

Similar work was done by Lee and Buss to adapt the virtual stiffness of a force-tracking impedance controller applied to a 7-DoF robotic manipulator [34]. The stiffness of the impedance model is varied over time as a function of both the end-effector's contact position and the measured force error signal. The influence stemming from the measured force error is computed as a proportional-derivative (PD) term with tunable gains. The authors numerically show that this proposed method is theoretically capable of keeping the steady-state force tracking errors below practical measurement resolutions despite cases of unknown environment parameters. Through simulations, the control scheme is demonstrated to track the desired applied force while traversing along the tangential direction of various walls. Multiple circumstances were analyzed including sharp changes in both wall geometry and wall stiffness. The controller demonstrates very rapid convergence, however it suffers from extremely high spike errors whenever the system experiences one of the sharp changes in the environment, such as a corner.

The limitations of the work by Lee and Buss were examined by Lu et al. where they employ a similar technique on a 2-DoF industrial manipulator [35]. As explained by the authors, the large instantaneous force errors experienced by Lee and Buss are due to the dependency of their adaptation law on the derivative of the force error. Though the implementation works very well with smooth interactions, it suffers greatly any time there is a rapid change in the error signal. For this reason, Lu et al. have modified the adaptation law to adjust the impedance stiffness matrix based on a differential-less method. Rather than looking at the force error itself, the modification presented in the paper defines the variable stiffness as the ratio of the desired force and the difference between the desired and commanded end-effector positions. The limitation of the paper is two-fold. Firstly, only simulation results are presented. And secondly, the stability of the adaptation law for the stiffness is only guaranteed under the assumption that the desired force and environment location are constant. This could be a limiting factor in the case of needing to initiate contact prior to tracing along the environment's surface.

As already seen, the adaptation of impedance control parameters can be accomplished in a number of ways. However, the performance of these methods can potentially be dependent on the noise experienced by the system, especially in cases where derivative terms are employed. Roveda and Piga have employed a way to vary both the stiffness and damping properties of an impedance controller so as to achieve different dynamic responses depending on how well the reference force is tracked [36]. Firstly, the variable stiffness is defined in such a way that it increases as the applied force approaches the desired reference signal. This is done by equating the stiffness to a nominal value minus the normalized force tracking error multiplied by a proportional gain. The reason for this variable stiffness definition is so that when the applied contact force is much different from that of the desired force (i.e. prior to contact, when the applied force is zero), the system is highly compliant. This allows the manipulator to more freely adjust as needed. As the force error approaches zero however, the system becomes stiffer, ensuring that the manipulator does not shift from its position. A similar approach is taken when defining the variable damping parameter. Like the stiffness, the system's behaviour is made to be such that it is less damp when the force error is large, meaning that the force tracking can be achieved much more rapidly. This is highly desirable especially when contact is first initiated. As the force error approaches zero, the damping ratio will increase in an effort to eliminate undesirable overshoots and oscillations. Simulations of this control methodology have shown its ability to rapidly converge to the desired contact force while resulting in low steady-state errors and no overshoot.

3.4.2. Vehicle Control

As it has been briefly touched upon already, the use of a decentralized control architecture would require methods to account for the influence of the robotic manipulator and its interaction with the environment. Since the vehicle's controller would have effectively no intended control of the end-effector control, the resulting external wrench can be treated as a disturbance to the vehicle body. Works in other fields have dealt with this concept and can be looked at for reference.

Simple vehicle control methods usually employ PID schemes to maintain tracking of positions and/or velocities. As described by Cieslak and Ridao however, this can become difficult when a floating platform attempts to apply significant forces to the environment as it becomes susceptible to noise, nonlinearities and time delays in the navigation control [33]. This can be greatly improved however if a priori knowledge of the wrench is available, as demonstrated by the authors on their work involving their autonomous underwater vehicle. The system is similar to the aerial manipulators discussed herein, where a robotic manipulator is integrated with the vehicle body, however its use case is for underwater pipe inspection. The authors explain that, even if the manipulator is performing the contact and controlling the wrench applied, in the steady-state, the resulting force must be counteracted by the vehicle thrust to keep the floating base steady. In the work, the desired wrench signal is passed directly to the vehicle body's thrust controller using feed-forward control. By doing so, the system is capable of anticipating the reaction forces which it would need to counter in order to keep the platform in a stable constant position.

An attempt to tackle this force/torque disturbance on the vehicle body is also analyzed by Giordano et al. on their design of a floating-base space robotic manipulator [37]. In their paper, they set requirements on the control architecture so that the vehicle's thrusters do not initiate contact and are only used to maintain the vehicle's body in place during the interaction. They do this by incorporating a so-called external/internal actuator allocation method. This allows them to compute the momentum of the system based on measured motion of the manipulator and vehicle body motion. This whole-body momentum is then fed back along with an estimate of the CoM and measure of the contact wrench to the external vehicle controller. It is worth noting that the feedback of the CoM allows the system to track a desired configuration of the robotic manipulator relative to the vehicle body, where the extent of this control can be tuned through a complimentary control gain. Results presented in the paper demonstrate that the vehicle is capable of floating freely through space just until contact is initiated, which is when the thrusters activate to accurately stabilize the vehicle.

3.5. Force Estimation

In order to implement an impedance control technique for contact-based interaction tasks, sufficient knowledge of the applied force is required. Many works involving manipulators typically employ sensors to measure the contact wrench. For example, a UAV with bottom-mounted robotic arm designed by Buzzatto et al. relies on a six-axis force/torque sensor which feeds the measurements directly to the vehicle's controller [38]. The issue with this approach though is that these sensors may physically interfere with other equipment, such as NDT sensors. Force/torque sensors also add additional weight to the drone, which may be unnecessary and should be avoided if possible. For these reasons, the following section will investigate force estimation techniques that have been employed throughout the literature for manipulation type tasks.

3.5.1. Momentum-Based External Force Estimator

The work by Ruggiero et al. discusses an interesting technique that aims to estimate the externally acting forces on a UAV [39]. This method is referred to as a momentum-based external generalized force estimator. It begins by introducing a generalized momentum vector which accounts for both the linear and angular momenta of the drone system. Using the system equations of motion, the time derivative of this generalized momentum vector can be computed. As discussed by the authors, the purpose of the estimator is to achieve a linear relationship between the estimated forces and their true values through a second-order Laplace function with desired natural frequency and damping parameter. The expression of this relationship in the time domain then calls on the use of the generalized momentum vector and its derivative that were previously introduced. Using this, an estimate of the external wrench can theoretically be computed through knowledge of the system dynamics.

Two different contributions by Bodie et al. implement this approach for the sake of contact-based inspections by aerial manipulators [1], [12]. In both works, the external wrench estimator is capable of yielding estimates of both the forces and torques experienced at the end-effectors of the manipulators using only measurements of the linear and angular velocities; no knowledge of the accelerations are required, meaning that the estimator is less susceptible to noise.

In [1] linear forces are estimated and validated against sensor measurements during omnidirectional contact of the end-effector with an arch. Large errors are seen in the estimation during initial contact with the surface due to the response of the estimator to a step input. These errors do reduce in magnitude, but still make up for a significant difference from the true applied forces. Estimation of the applied torques are not performed and it is noted that the estimator is not capable of differentiating between applied forces and ground/wall effects.

This work is extended in [12] where a six-axis force/torque sensor is added to the design. The system still utilizes the external wrench estimator, however here it is used only for the sake of estimating forces and torques that are unrelated to the interaction with the contact surface. The authors indicate that the method is not accurate enough to properly be used for the sake of intentional interaction control. Further, even if this method were to be used for interaction force tracking, the papers mentioned here have only applied it to the control of the vehicle's flight dynamics. There is clearly a need to implement a force tracking method for a decentralized manipulator which would be used directly for the interaction task.

3.5.2. Kalman Filtering

The Kalman filter, named after one of its developers, is an algorithm that using observations of noise-corrupted measurements along with the dynamics of a system model can accurately predict unknown variables of the system [40]. It does this by estimating a joint probability density of the system variables and by using this, can perform an update of the estimate based on a weighted dependency between the system dynamics and the measurements. This can prove to be quite useful for the sake of estimating the applied wrench at the end-effector of a manipulator. Most servo motors are capable of providing feedback of the measured joint torques experienced by the motors themselves. Using this along with the dynamics of the system could theoretically allow for the implementation of a Kalman filter to estimate the interaction forces and torques of the manipulator with the environment.

Along with their proposed adaptive impedance controller, Roveda and Piga have implemented a sensorless Extended Kalman Filter (EKF) to estimate the contact force at the manipulator's end-effector [36]. The estimator defines an augmented state vector consisting of both the end-effector's position and

velocity as well as the interaction force. The filter update dynamics are based upon the mass-spring-damper impedance model. The observer of the system transforms the joint positions and velocities to task-space values. Using this along with a noise vector to account for uncertainties attributed to each of the states, the authors could define the EKF algorithm to estimate the augmented state values, most importantly that of the interaction force. Validating this approach through simulation demonstrated that the estimated force nearly tracked the true applied force, with an error of about 6%. The major shortcoming of the work is that the method is only capable of estimating translational forces; there is room to expand the technique to obtain and estimate of the full wrench (i.e. including the torques applied at the end-effector).

A similar implementation can be seen in the work by Fakoorian et al. where they attempt to estimate the ground reaction forces of prosthetic legs [41]. The validity of the work can be easily related to that of aerial manipulators by considering the legs itself as the robotic manipulator making contact with the ground (rather than a wall) while being connected to a moving body. The system is even modelled using the mass-spring-damper equation for general robot dynamics. An augmented state vector is introduced that includes the angular position and angular velocities of each of the leg joints as well as the four reaction forces acting on the toe and heel. Using only measurements of the angular positions of the legs joints, an EKF is set up and is demonstrated to quickly converge to the true state values; thus correctly estimating the applied forces. As noted by the authors however, this approach requires the robot to be acting in a controlled setting where the environment parameters are sufficiently known. Further, convergence of the estimator is only guaranteed if the initial error is sufficiently small.

3.5.3. Other Methods

An alternative method to the EKF for estimating the applied wrench at the end-effector of a robotic manipulator is presented by Phong et al. [42]. Their work simultaneously employs a Time Delay Estimator (TDE) with a Simultaneous Input and State Estimator (SISE) to estimate the applied force without accurate knowledge of the interacting environment. The TDE portion of their algorithm works on the basis of modelling the dynamics of the system over a discrete time step with the external force as an unknown input to the system. The SISE algorithm employed is based on minimum unbiased variance estimation [43] that allows for the estimation of both the system states and unknown inputs even under the influence of non-Gaussian disturbances. The need for dealing with non-Gaussian disturbances is acknowledged by the authors for the reason that expected friction and backlash influences cannot be assumed to be Gaussian. Through both simulation and experimentation, the system is validated as it accurately tracks the applied force where a 4-DoF manipulator performs tasks involving the contact and wiping of a planar surface. Further work still needs to be done with this algorithm however to deal with non-planar surfaces as well as dynamically changing applied forces.

Alternatively, the robotic manipulation technique employed by Dong et al. utilizes the benefit of joint torque measurements to estimate the contact wrench at the end-effector [29]. From the general dynamic model of an n -DoF robot manipulator, the external joint torques can be expressed as a function of the measured internal joint torques and the general coordinates defining the joint motion. From these computed external joint torques, forward kinematics can be employed to determine the wrench applied at the end-effector. As noted by the authors however, the accelerations of the joints are often heavily corrupted by noise, making it difficult to directly compute the interaction wrench. For this reason, they have employed a third-order extended state observer (ESO) where the external applied joint torques are implicitly included in the augmented state and the only measurable states are the joint angular positions. Experimental validation of this method was performed where the estimate obtained from the ESO is compared with measurements made by an additional force sensor. The results show that over a range of applied force values from -50N to 50N , the ESO accurately tracks the true applied force with a mean error of about 0.48N . This method has only been implemented through simulation of a fixed-base industrial manipulator. Further research would be required to demonstrate its functionality in real-world experiments as well as on a floating base, such as an aerial manipulator.

3.6. Research Opportunity

This literature review has analyzed the different methods employed on various manipulation systems based on their potential contributions to a novel aerial manipulator for contact-based inspections. Each provides way to tackle a particular aspect of an aerial manipulation system, however there are clearly still some gaps which can be addressed. The following section will address the limitations of different contributions as a whole and aims to identify an opportunity for the proposed research.

On the topic of aerial manipulation, various physical designs were analyzed with differing implementations of manipulators on aerial vehicles. It was demonstrated that aerial manipulators could be categorized as either with or without active robotic manipulators. It was seen that even with the improved dexterity that is afforded by active manipulators, the reachable workspaces of most aerial manipulators are still quite limited due to physical limitations. Many bottom-mounted manipulators, such as the ones presented by Heredia et al. [22], Cataldi et al. [23], and Suarez et al. [24] introduce the requirement that drone approaches the target from above. In contrast, other works such as the system proposed by Markovic [26], have their manipulators mounted from above, but cannot interact with environments below them.

It was shown that there are available works pertaining to systems that claim omni-directional work spaces, however they tend to involve centralized control architecture with complex flight dynamics. Two such examples of this were presented in the works by Bodie et al. [1], [12] where fully-actuated UAV's were equipped with rigid booms and the reachability of the system stemmed purely from the motion control of the vehicle. Trujillo et al. [2] hinted at the possibility of attaining omni-directionality through the robotic manipulator as they centred their system around the CoM of the drone body with the ability to partially pivot about that point. Their system however lacks the capability to rotate the robotic manipulator entirely about the drone body, and hence relies heavily on the fully-actuated flight control of their tilt-rotor vehicle.

Based on this, it is evident that there is an opportunity to develop an aerial manipulator that offers an omni-directional workspace without needing to rely on extensive control of the vehicle's flight path and attitude. As discussed in the introduction, the proposed research will look to implement the conceptual design of Hamaza and Kovac [3] to accomplish this.

Along with this physical design, comes the need to establish control schemes that will allow the system to govern both the robotic manipulator and the aerial vehicle. It was demonstrated that decentralized control schemes allow the two controllers (one being for the robotic manipulator and the other being the flight controller) to be treated completely independently. Doing so however introduces the cases where the manipulator may reach its physical limitations, such as the maximum length which it can possibly extend, and so the system needs some method to account for this. As was shown in the work by Markovic et al. [26], control of the end-effector in inertial space can be allocated to the flight controller of a decoupled system when the robotic manipulator approaches these limitations. There is room to expand their methodology to be implemented on a robotic manipulator that offers full reachability around the entire drone body.

Continuing with this trend, gaps in the manipulator control methodologies can be identified next. As was discussed, the absence of knowledge around the intended task space, such as the contours which the end-effector would essentially need to follow, results in the preference toward impedance control schemes. Furthermore, if absolutely no knowledge of the environment parameters is available, then the implemented control scheme would effectively need to adjust in real time so that its dynamic response accounts for uncertainties. Adaptive impedance controllers have been implemented on both aerial and ground-fixed manipulators. Cieslak and Ridao [33] proposed adaptation laws based on the time integral of the wrench error for adjusting the stiffness matrix of the controller of their underwater manipulator, however it suffered from oscillatory behaviour when it attempted to apply desired forces on the environment. The adaptation laws by Lee and Buss [34] were implemented on a fixed-base industrial manipulator, however they were dependent on derivatives of the measured applied forces and thus suffered from inaccuracies when dealing with sharp changes in the environment. The method to adjust both the stiffness and damping properties of the impedance controller by Roveda and Piga [43] proved to be both intuitive and effective at maintaining desired contact forces with the environment while also dealing with the initiation and termination of contact. The method was developed for industrial manipulators however, and so there is an opportunity to expand its applicability to floating-base platforms such as an aerial manipulator. In doing so, inspiration can be pulled from the likes of Cieslak Ridao [33] or Giordano et al. [37] for methods to stabilize the aerial platform during contact of its end-effector with

the environment by treating the induced reactionary wrench as an external disturbance. The methods have been proven for underwater vehicles and spacecraft respectively. The implementation of either one, either using an external wrench feed-forward signal or using external/internal actuator allocation, would be essential to ensuring stability of the decentralized system during environment interaction.

Finally, wrench estimation techniques presented in the literature were analyzed as there is a desire to avoid the use of additional force/torque sensors at the end-effector. For this, different approaches were looked at. These included the momentum-based estimators by Bodie et al. [1], [12], the extended Kalman filters by Roveda & Piga [36] and Fakoorian et al. [41], the time delay estimator by Phong et al. [42], and the extended state observer based on measure joint torques by Dong et al. [29]. Of all the cases presented, only the work by Bodie et al. was implemented on an omni-directional aerial manipulator; the others were implemented on static-base industrial manipulators. Further, the momentum-based estimator by Bodie et al. was shown to be inadequate for estimating contact forces through the manipulator. As such, there is an opportunity to implement something along the lines of the extended state observer with joint torque feedback directly on an aerial manipulator.

To summarize the research gaps presented herein, one could look at two general areas. Firstly, to the extent of what could be found for this literature review, there is currently no aerial manipulator with an omni-directional workspace that does not rely directly on flight control to achieve this reachability. As discussed earlier on, only a concept design has been put forth by Hamaza and Kovac [3]; and it is intended that this concept be pursued for this proposed research. Secondly, though each of the system aspects discussed throughout this report have been researched to varying extents, there is currently no implementation that consolidates them all into one system. To be specific, there does not seem to be an aerial manipulator with a decentralized control architecture which implements sensorless adaptive impedance control using force estimation.

3.7. Conclusion

To conclude this report, the research question that was posed in the introduction is revisited along with the corresponding sub-questions. Recalling, the proposed research aims to determine how accurately an aerial manipulator could apply a desired wrench on an environment's surface through its end-effector while traversing the contour of this surface. Two qualifying conditions were also imposed on this research question. Firstly, the system is expected to have no knowledge of the environment, both in terms of shape and surface properties. Secondly, the system is expected not to rely on direct force/torque measurements through the use of a sensor at the end-effector. In order for the proposed research to properly answer this question, a number of sub-questions were laid out to break down the low-level objectives which the research must pursue.

The first question aimed to look into the integration of the two subsystems, the aerial vehicle and the robotic manipulator, along with how control allocation could be efficiently shared between the two. The review delved into works regarding both centralized and decentralized approaches, demonstrating the ability through the latter to completely decouple end-effector control from the vehicle flight control. Along with this decoupled system architecture, it was noted that the issue of singularities in the manipulator configuration could be experienced. To account for this, methodology was reviewed that yields control to the vehicle controller so that the manipulator does not reach these singularities.

Secondly, since the research question ponders the effectiveness of interaction control without direct force/torque sensors, it was noted that it is critical to measure how accurately the system could estimate the applied wrench. Multiple approaches to force estimation were discussed and it was noted that though most could accurately estimate the applied forces and torques, the implementations in the literature were employed on static-base manipulators. A research gap was identified pertaining to the lack of accurate force estimation schemes employed on aerial manipulators that are capable of estimating the force induced by environment interaction.

The final sub-question that was defined pertained to the vehicle's motion amid interaction with the environment. To recall, we wish to measure how well the intended flight trajectory could be maintained while applying contact forces. Under a decentralized system, these forces would effectively act as disturbances which would need to be counteracted. Methodologies that pertained to providing the flight controller with information regarding these contact forces and torques were analyzed. It was noted however that though they have been implemented on other floating-base platforms, little work has gone into using these methods aboard aerial manipulators.

With each of these research areas analyzed, the general opportunity for a research contribution was then finally provided. It was found that though there exists extensive research for each of the primary sub-tasks discussed, there is no evidence of a system that integrates each of these sub-tasks to achieve a truly decentralized, omni-directional aerial manipulator. Thus tying back to the initial discussion on NDT, the goal of the proposed research will be to prove that consistent contact-based force tracking can be achieved without knowledge of the environment nor the use of force/torque sensors. This will effectively pave the way for a system which could be deployed to various infrastructures to perform tests, which would otherwise place human operators in dangerous and/or difficult to reach areas.

References

- [1] K. Bodie, M. Brunner, M. Pantic, *et al.*, “An omnidirectional aerial manipulation platform for contact-based inspection,” *Robotics: Science and Systems XV*, Jun. 22, 2019. DOI: 10.15607/RSS.2019.XV.019. arXiv: 1905.03502.
- [2] M. Á. Trujillo, J. R. Martínez-de Dios, C. Martín, A. Viguria, and A. Ollero, “Novel aerial manipulator for accurate and robust industrial NDT contact inspection: A new tool for the oil and gas inspection industry,” *Sensors*, vol. 19, no. 6, p. 1305, Jan. 2019, Number: 6 Publisher: Multidisciplinary Digital Publishing Institute. DOI: 10.3390/s19061305.
- [3] S. Hamaza and M. Kovac, “Omni-drone: On the design of a novel aerial manipulator with omnidirectional workspace,” in *2020 17th International Conference on Ubiquitous Robots (UR)*, ISSN: 2325-033X, Jun. 2020, pp. 153–158. DOI: 10.1109/UR49135.2020.9144837.
- [4] F. Ruggiero, V. Lippiello, and A. Ollero, “Aerial manipulation: A literature review,” *IEEE Robotics and Automation Letters*, vol. 3, no. 3, pp. 1957–1964, 2018.
- [5] S. Gholizadeh, “A review of non-destructive testing methods of composite materials,” *Procedia Structural Integrity*, vol. 1, pp. 50–57, 2016.
- [6] C. Mineo, D. Herbert, M. Morozov, S. Pierce, P. Nicholson, and I. Cooper, “Robotic non-destructive inspection,” in *51st Annual Conference of the British Institute of Non-Destructive Testing*, 2012, pp. 345–352.
- [7] R. Bogue, “The role of robotics in non-destructive testing,” *Industrial Robot: An International Journal*, 2010.
- [8] M. Car, L. Markovic, A. Ivanovic, M. Orsag, and S. Bogdan, “Autonomous wind-turbine blade inspection using LiDAR-equipped unmanned aerial vehicle,” *IEEE Access*, vol. 8, pp. 131 380–131 387, 2020, Conference Name: IEEE Access, ISSN: 2169-3536. DOI: 10.1109/ACCESS.2020.3009738.
- [9] D. Zhang, R. Watson, G. Dobie, C. MacLeod, and G. Pierce, “Autonomous ultrasonic inspection using unmanned aerial vehicle,” in *2018 IEEE International Ultrasonics Symposium (IUS)*, ISSN: 1948-5727, Oct. 2018, pp. 1–4. DOI: 10.1109/ULTSYM.2018.8579727.
- [10] S. Hamaza, I. Georgilas, and T. Richardson, “2d contour following with an unmanned aerial manipulator: Towards tactile-based aerial navigation,” in *2019 IEEE/RSJ International Conference on Intelligent Robots and Systems (IROS)*, ISSN: 2153-0866, Nov. 2019, pp. 3664–3669. DOI: 10.1109/IROS40897.2019.8968591.
- [11] X. Meng, Y. He, and J. Han, “Design and implementation of a contact aerial manipulator system for glass-wall inspection tasks,” in *2019 IEEE/RSJ International Conference on Intelligent Robots and Systems (IROS)*, ISSN: 2153-0866, Nov. 2019, pp. 215–220. DOI: 10.1109/IROS40897.2019.8968123.
- [12] K. Bodie, M. Brunner, M. Pantic, *et al.*, “Active interaction force control for contact-based inspection with a fully actuated aerial vehicle,” *IEEE Transactions on Robotics*, vol. 37, no. 3, pp. 709–722, Jun. 2021, Conference Name: IEEE Transactions on Robotics, ISSN: 1941-0468. DOI: 10.1109/TR0.2020.3036623.
- [13] T. Bartelds, A. Capra, S. Hamaza, S. Stramigioli, and M. Fumagalli, “Compliant aerial manipulators: Toward a new generation of aerial robotic workers,” *IEEE Robotics and Automation Letters*, vol. 1, no. 1, pp. 477–483, Jan. 2016, Conference Name: IEEE Robotics and Automation Letters, ISSN: 2377-3766. DOI: 10.1109/LRA.2016.2519948.
- [14] D. Mellinger, Q. Lindsey, M. Shomin, and V. Kumar, “Design, modeling, estimation and control for aerial grasping and manipulation,” in *2011 IEEE/RSJ International Conference on Intelligent Robots and Systems*, ISSN: 2153-0866, Sep. 2011, pp. 2668–2673. DOI: 10.1109/IROS.2011.6094871.

- [15] D. Smrcka, T. Baca, T. Nascimento, and M. Saska, "Admittance force-based UAV-wall stabilization and press exertion for documentation and inspection of historical buildings," in *2021 International Conference on Unmanned Aircraft Systems (ICUAS)*, ISSN: 2575-7296, Jun. 2021, pp. 552–559. DOI: 10.1109/ICUAS51884.2021.9476873.
- [16] H.-N. Nguyen and D. Lee, "Hybrid force/motion control and internal dynamics of quadrotors for tool operation," in *2013 IEEE/RSJ International Conference on Intelligent Robots and Systems*, ISSN: 2153-0866, Nov. 2013, pp. 3458–3464. DOI: 10.1109/IR0S.2013.6696849.
- [17] F. Huber, K. Kondak, K. Krieger, *et al.*, "First analysis and experiments in aerial manipulation using fully actuated redundant robot arm," in *2013 IEEE/RSJ International Conference on Intelligent Robots and Systems*, ISSN: 2153-0866, Nov. 2013, pp. 3452–3457. DOI: 10.1109/IR0S.2013.6696848.
- [18] S. Kim, S. Choi, and H. J. Kim, "Aerial manipulation using a quadrotor with a two DOF robotic arm," in *2013 IEEE/RSJ International Conference on Intelligent Robots and Systems*, ISSN: 2153-0866, Nov. 2013, pp. 4990–4995. DOI: 10.1109/IR0S.2013.6697077.
- [19] M. Tognon, B. Yüksel, G. Buondonno, and A. Franchi, "Dynamic decentralized control for proto-centric aerial manipulators," in *2017 IEEE International Conference on Robotics and Automation (ICRA)*, May 2017, pp. 6375–6380. DOI: 10.1109/ICRA.2017.7989753.
- [20] J. Thomas, J. Polin, K. Sreenath, and V. Kumar, "Avian-inspired grasping for quadrotor micro UAVs," in *Volume 6A: 37th Mechanisms and Robotics Conference*, Portland, Oregon, USA: American Society of Mechanical Engineers, Aug. 4, 2013, V06AT07A014, ISBN: 978-0-7918-5593-5. DOI: 10.1115/DETC2013-13289.
- [21] R. Peng, X. Chen, and P. Lu, "A motion decoupled aerial robotic manipulator for better inspection," in *2021 IEEE/RSJ International Conference on Intelligent Robots and Systems (IROS)*, ISSN: 2153-0866, Sep. 2021, pp. 4207–4213. DOI: 10.1109/IR0S51168.2021.9636765.
- [22] G. Heredia, A. Jimenez-Cano, I. Sanchez, *et al.*, "Control of a multirotor outdoor aerial manipulator," in *2014 IEEE/RSJ International Conference on Intelligent Robots and Systems*, ISSN: 2153-0866, Sep. 2014, pp. 3417–3422. DOI: 10.1109/IR0S.2014.6943038.
- [23] E. Cataldi, G. Muscio, M. A. Trujillo, *et al.*, "Impedance control of an aerial-manipulator: Preliminary results," in *2016 IEEE/RSJ International Conference on Intelligent Robots and Systems (IROS)*, ISSN: 2153-0866, Oct. 2016, pp. 3848–3853. DOI: 10.1109/IR0S.2016.7759566.
- [24] A. Suarez, G. Heredia, and A. Ollero, "Physical-virtual impedance control in ultralightweight and compliant dual-arm aerial manipulators," *IEEE Robotics and Automation Letters*, vol. 3, no. 3, pp. 2553–2560, Jul. 2018, Conference Name: IEEE Robotics and Automation Letters, ISSN: 2377-3766. DOI: 10.1109/LRA.2018.2809964.
- [25] M. Tognon, H. A. T. Chávez, E. Gasparin, *et al.*, "A truly-redundant aerial manipulator system with application to push-and-slide inspection in industrial plants," *IEEE Robotics and Automation Letters*, vol. 4, no. 2, pp. 1846–1851, Apr. 2019, Conference Name: IEEE Robotics and Automation Letters, ISSN: 2377-3766. DOI: 10.1109/LRA.2019.2895880.
- [26] L. Marković, M. Car, M. Orsag, and S. Bogdan, "Adaptive stiffness estimation impedance control for achieving sustained contact in aerial manipulation," in *2021 IEEE International Conference on Robotics and Automation (ICRA)*, ISSN: 2577-087X, May 2021, pp. 117–123. DOI: 10.1109/ICRA48506.2021.9561886.
- [27] L. Villani and J. De Schutter, "Force control," in *Springer Handbook for Robotics*, 2nd ed., Berlin: Springer, 2016, pp. 195–220.
- [28] M. H. Raibert and J. J. Craig, "Hybrid position/force control of manipulators," *Journal of Dynamic Systems, Measurement, and Control*, vol. 103, no. 2, pp. 126–133, Jun. 1, 1981, ISSN: 0022-0434, 1528-9028. DOI: 10.1115/1.3139652.
- [29] Y. Dong, T. Ren, K. Hu, D. Wu, and K. Chen, "Contact force detection and control for robotic polishing based on joint torque sensors," *The International Journal of Advanced Manufacturing Technology*, vol. 107, no. 5, pp. 2745–2756, Mar. 2020, ISSN: 0268-3768, 1433-3015. DOI: 10.1007/s00170-020-05162-8.

- [30] S. Xu, B. He, Y. Zhou, Z. Wang, and C. Zhang, "A hybrid position/force control method for a continuum robot with robotic and environmental compliance," *IEEE Access*, vol. 7, pp. 100467–100479, 2019, Conference Name: IEEE Access, ISSN: 2169-3536. DOI: 10.1109/ACCESS.2019.2928572.
- [31] F. Jatta, G. Legnani, A. Visioli, and G. Ziliani, "On the use of velocity feedback in hybrid force/velocity control of industrial manipulators," *Control Engineering Practice*, vol. 14, no. 9, pp. 1045–1055, Sep. 1, 2006, ISSN: 0967-0661. DOI: 10.1016/j.conengprac.2005.06.005.
- [32] M. Car, A. Ivanovic, M. Orsag, and S. Bogdan, "Position-based adaptive impedance control for a UAV," in *2018 International Conference on Unmanned Aircraft Systems (ICUAS)*, ISSN: 2575-7296, Jun. 2018, pp. 957–963. DOI: 10.1109/ICUAS.2018.8453397.
- [33] P. Cieślak and P. Ridao, "Adaptive admittance control in task-priority framework for contact force control in autonomous underwater floating manipulation," in *2018 IEEE/RSJ International Conference on Intelligent Robots and Systems (IROS)*, ISSN: 2153-0866, Oct. 2018, pp. 6646–6651. DOI: 10.1109/IROS.2018.8593542.
- [34] K. Lee and M. Buss, "Force tracking impedance control with variable target stiffness," *IFAC Proceedings Volumes*, 17th IFAC World Congress, vol. 41, no. 2, pp. 6751–6756, Jan. 1, 2008, ISSN: 1474-6670. DOI: 10.3182/20080706-5-KR-1001.01144.
- [35] W. Lu, H. Liu, X. Zhu, X. Wang, and B. Liang, "Variable stiffness force tracking impedance control using differential-less method," in *2017 29th Chinese Control And Decision Conference (CCDC)*, ISSN: 1948-9447, May 2017, pp. 4906–4911. DOI: 10.1109/CCDC.2017.7979364.
- [36] L. Roveda and D. Piga, "Sensorless environment stiffness and interaction force estimation for impedance control tuning in robotized interaction tasks," *Autonomous Robots*, vol. 45, no. 3, pp. 371–388, Mar. 2021, ISSN: 0929-5593, 1573-7527. DOI: 10.1007/s10514-021-09970-z.
- [37] A. M. Giordano, D. Calzolari, M. De Stefano, H. Mishra, C. Ott, and A. Albu-Schäffer, "Compliant floating-base control of space robots," *IEEE Robotics and Automation Letters*, vol. 6, no. 4, pp. 7485–7492, Oct. 2021, Conference Name: IEEE Robotics and Automation Letters, ISSN: 2377-3766. DOI: 10.1109/LRA.2021.3097496.
- [38] J. Buzzato, A. Hernandez, M. Becker, and G. d. P. Caurin, "Aerial manipulation with six-axis force and torque sensor feedback compensation," in *2018 Latin American Robotic Symposium, 2018 Brazilian Symposium on Robotics (SBR) and 2018 Workshop on Robotics in Education (WRE)*, Nov. 2018, pp. 158–163. DOI: 10.1109/LARS/SBR/WRE.2018.00037.
- [39] F. Ruggiero, J. Cacace, H. Sadeghian, and V. Lippiello, "Impedance control of VTOL UAVs with a momentum-based external generalized forces estimator," in *2014 IEEE International Conference on Robotics and Automation (ICRA)*, ISSN: 1050-4729, May 2014, pp. 2093–2099. DOI: 10.1109/ICRA.2014.6907146.
- [40] R. E. Kalman, "A new approach to linear filtering and prediction problems," *Journal of Basic Engineering*, vol. 82, no. 1, pp. 35–45, Mar. 1, 1960, ISSN: 0021-9223. DOI: 10.1115/1.3662552.
- [41] S. Fakoorian, V. Azimi, M. Moosavi, H. Richter, and D. Simon, "Ground reaction force estimation in prosthetic legs with nonlinear kalman filtering methods," *Journal of Dynamic Systems, Measurement, and Control*, vol. 139, no. 11, Jul. 20, 2017, ISSN: 0022-0434. DOI: 10.1115/1.4036546.
- [42] L. D. Phong, J. Choi, W. Lee, and S. Kang, "A novel method for estimating external force: Simulation study with a 4-DOF robot manipulator," *International Journal of Precision Engineering and Manufacturing*, vol. 16, no. 4, pp. 755–766, Apr. 2015, ISSN: 2234-7593, 2005-4602. DOI: 10.1007/s12541-015-0100-7.
- [43] L. Roveda and D. Piga, "Robust state dependent riccati equation variable impedance control for robotic force-tracking tasks," *International Journal of Intelligent Robotics and Applications*, vol. 4, no. 4, pp. 507–519, Dec. 2020, ISSN: 2366-5971, 2366-598X. DOI: 10.1007/s41315-020-00153-0.